An MsFEM type approach for perforated domains

Claude Le Bris[1], Frédéric Legoll[1], Alexei Lozinski[2]

[1] École Nationale des Ponts et Chaussées,

6 et 8 avenue Blaise Pascal, 77455 Marne-La-Vallée Cedex 2, FRANCE

and

INRIA Rocquencourt, MICMAC project-team,

78153 Le Chesnay Cedex, FRANCE

`lebris@cermics.enpc.fr, legoll@lami.enpc.fr`

[2] Formerly at Institut de Mathématiques de Toulouse,

Université Paul Sabatier,

118 route de Narbonne, 31062 Toulouse Cedex 9, FRANCE

Now at Laboratoire de Mathématiques CNRS UMR 6623,

Université de Franche-Comté, 16 route de Gray, 25030 Besançon Cedex, FRANCE

`alexei.lozinski@univ-fcomte.fr`

October 29, 2018

Abstract

We follow up on our previous work [21] where we have studied a multiscale finite element (MsFEM) type method in the vein of the classical Crouzeix-Raviart finite element method that is specifically adapted for highly oscillatory elliptic problems. We adapt the approach to address here a multiscale problem on a perforated domain. An additional ingredient of our approach is the enrichment of the multiscale finite element space using bubble functions. We first establish a theoretical error estimate. We next show that, on the problem we consider, the approach we propose outperforms all dedicated existing variants of MsFEM we are aware of.

1

1 Introduction

1.1 Generalities

We consider a bounded domain $\Omega \subset \mathbb{R}^d$ and a set B_ε of perforations within this domain. The perforations are supposedly small and in extremely large a number. The parameter ε stands here for a typical distance between the perforations. We denote by $\Omega_\varepsilon = \Omega \backslash \overline{B_\varepsilon}$ the perforated domain (see Figure 1). We then consider the following problem: find $u : \Omega_\varepsilon \to \mathbb{R}$, solution of

$$- \Delta u = f \text{ in } \Omega_\varepsilon, \quad u = 0 \text{ on } \partial\Omega_\varepsilon, \tag{1}$$

where $f : \Omega \to \mathbb{R}$ is a given function, assumed sufficiently regular on Ω. It is important to note that the homogeneous Dirichlet boundary condition on $\partial\Omega_\varepsilon$ (and hence on the boundary $\Omega \cap \partial B_\varepsilon$ of the perforations) is a crucial feature of the problem we consider. Our academic enterprise is motivated by various physically relevant problems, for instance in fluid mechanics, atmospheric modeling, electrostatic devices, ... A different boundary condition, such as a Neumann boundary condition, would lead to completely different theoretical considerations and, eventually, a different numerical approach. The consideration of (1) can also be seen as a step toward the resolution of the Stokes problem on perforated domains. In that latter case, homogeneous Dirichlet boundary conditions on the perforations are typical for many applicative contexts.
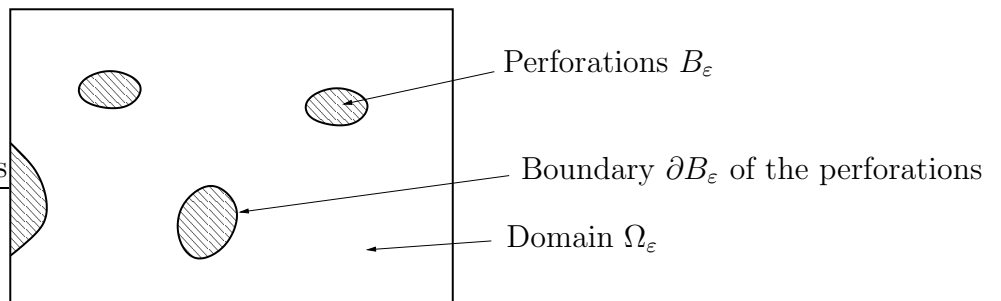
Figure 1: The domain Ω contains perforations B_ε. The perforated domain is $\Omega_\varepsilon = \Omega \setminus \overline{B_\varepsilon}$. The boundary of Ω_ε is the union of $\partial B_\varepsilon \cap \overline{\Omega_\varepsilon}$ (the part of the boundary of the perforations that is included in $\overline{\Omega_\varepsilon}$) and of $\partial\Omega \cap \overline{\Omega_\varepsilon}$.

Our purpose here is to propose and study a dedicated multiscale finite element method (MsFEM). To this end, we consider the variant of MsFEM

2

using *Crouzeix-Raviart type* finite elements [9] which we have employed and studied for a prototypical multiscale elliptic problem in [21] and we adapt the approach for the particular setting under consideration here. The major adaptation we perform (and thus one of the added values with respect to our earlier work [21]) is the addition of *bubble functions* to the finite element basis set. Let us briefly comment upon the motivation for these two ingredients: Crouzeix-Raviart type finite element on the one hand, and addition of bubble functions on the other hand.

The motivation for using Crouzeix-Raviart type finite elements stems from our wish to devise a numerical approach as accurate as possible for a limited computational workload. In general, it is well known that, for the construction of multiscale finite elements, boundary conditions set on the edges (facets) of mesh elements for the definition of the basis functions play a critical role for the eventual accuracy and efficiency of the approach. Using Crouzeix-Raviart type elements (see [9] for their original introduction) gives a definite flexibility. In short, the continuity of our multiscale finite element basis set functions accross the edges of the mesh is enforced only in a weak sense by requiring that the average of the jump vanishes on each edge. This "weak" continuity condition leads to some natural boundary conditions for the multiscale basis functions (see Section 2.1). The nonconforming approximation obtained in this manner proves to be very effective, see [21]. The above issue regarding boundary conditions on the mesh elements is all the more crucial when dealing with perforated computational domains. Indeed, we want the approach we construct to be as insensitive as possible to the possible intersections between element edges and perforations. The long term motivation for this is the wish to address problems where the perforations can be very heterogeneously distributed (think, say, of nonperiodic, or even random arrays of perforations). The *ad hoc* construction of a mesh that (essentially) avoids intersecting the perforations is then prohibitively difficult.

The second ingredient of our approach is the addition of bubble functions to the finite element space. As illustrated using a simple one-dimensional analysis in Section 1.2, and demonstrated with an extensive set of numerical tests in Section 5 for all MsFEM type approches we implemented, the addition of bubble functions is definitely benefitial for the overall accuracy of the approach.

The literature on the types of problems and techniques considered here is of course too vast to be recalled here. A quite general review is contained

in our earlier work [21]. We however wish to mention here the references [2, 10] for the general background on MsFEM, and the works [6, 7, 8, 16, 17, 22] specifically addressing problems on perforated domains, either from a theoretical or a numerical standpoint.

The outline of our article is as follows. As already briefly mentioned, the rest of this introduction, namely Section 1.2, is devoted to the study of a simple one-dimensional situation. From Section 2 on, we work in two dimensions throughout the article, both for the analysis and for the numerical tests of the final section. We however emphasize that, of course, the approach can be applied to the three-dimensional context and that, most likely, the theoretical analysis we provide here can also be extended to the three dimensional case (Note that our analysis in [21] was performed in both the two and three dimensional settings). We will not proceed in this direction here. In addition and for simplicity, we assume that Ω is a polygonal domain. Section 2 presents our finite element approach and the main result of numerical analysis (Theorem 4) we are able to prove, under restrictive assumptions made precise below (in particular, periodicity of the perforations is assumed, although, in practice, the approach is *not* restricted to this setting). Section 3 prepares the ground for the proof of this main result, performed in Section 4. Our final Section 5 then presents a comprehensive set of numerical experiments. When using our MsFEM approach on a perforated domain, there are essentially three "parameters": (i) the boundary conditions imposed to define the MsFEM basis functions, (ii) the addition, or not, of bubble functions and (iii) the possible intersections of the perforations with the edges (facets) of mesh elements. Assessing the validity of our approach requires to compare it with the other existing approaches for all possible combinations of the above three "parameters". This is what we complete in Section 5. Our tests demonstrate that the combination of Crouzeix-Raviart type finite elements and bubble functions allows to outperform all the other existing approaches on the problem considered here in a way that is essentially insensitive to intersections of the mesh with the perforations.

1.2 A one-dimensional situation

In order to illustrate the specificity of multiscale perforated problems, and to already discover some interesting features, we first consider an academic one-dimensional setting. Consider the one-dimensional version of the boundary

value problem (1) for $\Omega = (0, L)$, B_ε the set of segments $B_\varepsilon = \cup_{j=1}^J (a_j, b_j)$ with $0 < a_1 < b_1 < a_2 < b_2 < \cdots < L$. We suppose that the gaps between the perforations are of length at most ε, that is $a_1 \leq \varepsilon$, $a_2 - b_1 \leq \varepsilon$, $a_3 - b_2 \leq \varepsilon$, ..., $L - b_J \leq \varepsilon$. Other than that, we do not put any assumption on the geometry of these one-dimensional perforations. Note that in particular (and in contrast to the analysis we perform later on in this article) we do *not* assume any periodicity of the perforations. The weak form of our problem then reads: find $u \in H_0^1(\Omega_\varepsilon)$ such that

$$\forall v \in H_0^1(\Omega_\varepsilon), \quad a(u, v) = \int_{\Omega_\varepsilon} fv, \tag{2}$$

where, we recall, $\Omega_\varepsilon = \Omega \setminus B_\varepsilon$ denotes the perforated domain and where

$$a(u, v) = \int_{\Omega_\varepsilon} u' \, v'.$$

We now divide Ω into N segments $K_i = [x_{i-1}, x_i]$, $i = 1, \ldots, N$, by the nodes $0 = x_0 < x_1 < \cdots < x_N = L$, define the mesh size $H = \max |x_i - x_{i-1}|$, and consider the multiscale finite element space adapted to the perforated domain

$$V_H = \left\{ \begin{array}{c} u_H \in C^0(\Omega) \text{ such that } u_H = 0 \text{ on } B_\varepsilon \cup \partial\Omega \text{ and} \\ u_H'' = C_i \text{ in } K_i \cap \Omega_\varepsilon, \, i = 1, \ldots, N, \text{ for some constants } C_i \end{array} \right\}.$$

Note that the domain $K_i \cap \Omega_\varepsilon$ may be not connected. We nevertheless assume that u_H'' is equal to the *same* constant C_i on all the connected components of $K_i \cap \Omega_\varepsilon$.

Remark 1. *In the one-dimensional setting, the Crouzeix-Raviart type boundary condition that we consider in this work simply amounts to a continuity condition at the mesh nodes. This is why we require that $u_H \in C^0(\Omega)$ in the above definition of V_H. This observation holds for many variants of MsFEM, including the oversampling variant, which, alike the Crouzeix-Raviart variant we introduce here, uses non-conforming finite elements. In this respect, the one-dimensional setting is not typical.*

The Galerkin approximation of the solution to problem (2) is then introduced as the solution $u_H \in V_H$ to

$$\forall v_H \in V_H, \quad a(u_H, v_H) = \int_{\Omega_\varepsilon} fv_H. \tag{3}$$

Readers familiar with the MsFEM approach will notice that V_H contains more functions than the usual MsFEM basis set, which would consist here in taking $u''_H = 0$ (rather than an arbitrary constant C_i) on $K_i \cap \Omega_\varepsilon$.

A convenient generating family for the space V_H may be constructed as follows. First we associate a function Φ_i to any internal node x_i by solving

$$
\begin{aligned}
\operatorname{supp} \Phi_i &\subset (x_{i-1}, x_{i+1}), \\
\Phi''_i &= 0 \text{ in } (x_{i-1}, x_i) \cap \Omega_\varepsilon \text{ and in } (x_i, x_{i+1}) \cap \Omega_\varepsilon, \\
\Phi_i &= 0 \text{ in } B_\varepsilon, \\
\Phi_i(x_i) &= 1 \text{ if } x_i \in \Omega_\varepsilon \text{ or } 0 \text{ otherwise.}
\end{aligned}
$$

Note that this construction yields $\Phi_i \equiv 0$ if the node x_i lies inside a perforation (see Fig. 2). Second, we associate a function Ψ_i to any segment $K_i = [x_{i-1}, x_i]$ by solving (see Fig. 3)

$$
\begin{aligned}
\operatorname{supp} \Psi_i &\subset (x_{i-1}, x_i), \\
-\Psi''_i &= 1 \text{ in } K_i \cap \Omega_\varepsilon, \\
\Psi_i &= 0 \text{ in } B_\varepsilon.
\end{aligned}
$$

The functions Φ_i $(1 \le i \le N - 1)$ and Ψ_j $(1 \le j \le N)$ are linearly independent (except for the trivial case when $\Phi_i \equiv 0$), and we obviously have

$$
\operatorname{span} \{\Phi_1, \ldots, \Phi_{N-1}, \Psi_1, \ldots, \Psi_N\} \subset V_H.
$$

In turn, any $u \in V_H$ can be written $u = \sum_{j=1}^{N} C_j \Psi_j + \sum_{i=1}^{N-1} u(x_i) \Phi_i$. We thus have

$$
V_H = \operatorname{span} \{\Phi_1, \ldots, \Phi_{N-1}, \Psi_1, \ldots, \Psi_N\},
$$

which implies that the space V_H is of dimension at most $2N - 1$.
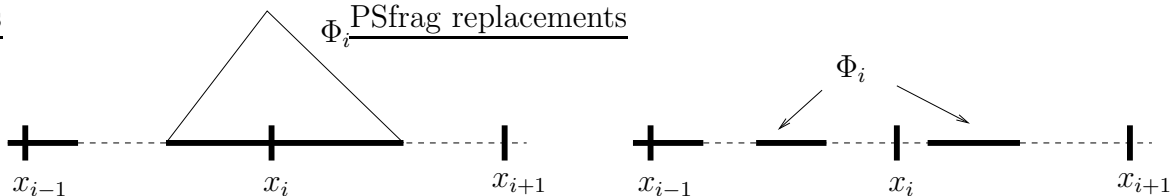
Figure 2: Basis function Φ_i (Solid line: domain Ω_ε; dashed line: perforations B_ε). Left: case when $x_i \in \Omega_\varepsilon$. Right: case when $x_i \notin \Omega_\varepsilon$, for which $\Phi_i \equiv 0$.
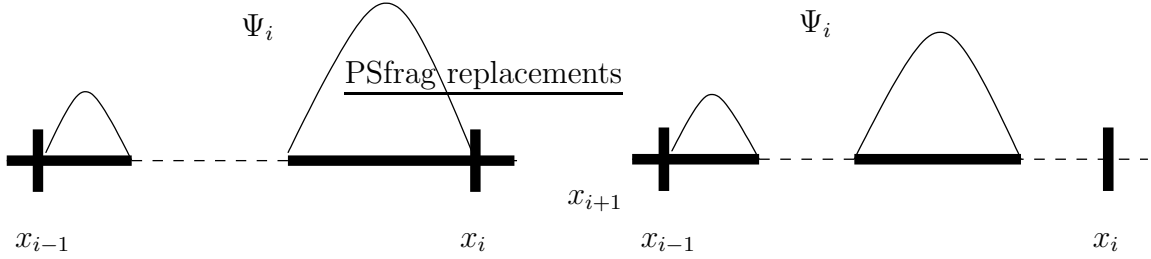
Figure 3: Basis function Ψ_i (Solid line: domain Ω_ε; dashed line: perforations B_ε). Left: case when $x_i \in \Omega_\varepsilon$. Right: case when $x_i \notin \Omega_\varepsilon$. In both cases, $\Psi_i \neq 0$.

It is interesting to note that the functions Ψ_i, which act as *bubble functions*, are necessary to generate an efficient approximation space. The reason is evident in the one-dimensional situation, since, in the absence of such a bubble (or of a basis function playing a similar role), there is no way to recover a good approximation quality between two consecutive perforations if no node is actually present there. The numerical solution would systematically vanish in such a region (see Fig. 2, right part). In higher dimensions, the phenomenon is less accute (since perforations, unless of a particular shape, cannot isolate regions of the space from the neighborhood) but it is still, to some extent, relevant. We will observe the definite added value of bubble functions in our numerical tests of Section 5.

We then have the following (simple) numerical analysis result.

Theorem 2. *Assume that the right-hand side f in (2) satisfies $f \in H^1(\Omega)$. Then the Galerkin solution u_H of (3) satisfies the error estimate*

$$|u - u_H|_{H^1(\Omega_\varepsilon)} \leq C\varepsilon H \|f'\|_{L^2(\Omega)}, \tag{4}$$

where $|\cdot|_{H^1(\Omega_\varepsilon)}$ is the energy norm associated to the bilinear form a:

$$\forall v \in H^1(\Omega_\varepsilon), \quad |v|_{H^1(\Omega_\varepsilon)} := \sqrt{a(v,v)} = \sqrt{\int_{\Omega_\varepsilon} (v')^2}.$$

The factor ε in the right-hand side of (4) needs to be understood as follows. It turns out that, for the category of problems (1) we consider, the exact solution u (and thus, correspondingly, its numerical approximation u_H)

7

is of size ε in H^1 norm for ε small, as is proved by homogenization theory and will be recalled –for the periodic setting– in Section 3.1 below (see (18) and (21)). Once this scale factor is accounted for, the estimate (4) shows that the numerical approach is first order accurate in the meshsize H, with a prefactor $C \, \|f'\|_{L^2(\Omega)}$ that is *independent* of the size ε of the geometric oscillations.

Proof. We see from (2) and (3) that

$$\forall v_H \in V_H, \quad a(u - u_H, v_H) = 0.$$

Consequently, u_H is the orthogonal projection of u on V_H, where by *orthogonality* we mean orthogonality for the scalar product defined by the bilinear form a. We therefore have

$$|u - u_H|_{H^1(\Omega_\varepsilon)} = \inf_{v_H \in V_H} |u - v_H|_{H^1(\Omega_\varepsilon)}. \tag{5}$$

Proving (4) therefore amounts to proving the inequality for at least one function $v_H \in V_H$. We take $v_H \in V_H$ such that $v_H(x_i) = u(x_i)$, $i = 0, 1, \ldots, N$, and $-v_H'' = \Pi_H f$ on each $K_i \cap \Omega_\varepsilon$, where $\Pi_H f$ is the L^2-orthogonal projection of f on the space of piecewise constant functions. Consider then the interpolation error $e = u - v_H$. We remark that

$$\begin{cases} -e'' = f - \Pi_H f \ \text{ on each } (x_{j-1}, x_j) \cap \Omega_\varepsilon, \quad 1 \leq j \leq N, \\ e(x_j) = 0, \quad j = 0, \ldots, N. \end{cases}$$

Denoting by $b_0 = 0$ and $a_{J+1} = L$, we have

$$|e|^2_{H^1(\Omega_\varepsilon)} = \int_{\Omega_\varepsilon} |e'|^2 = \sum_{j=0}^{J} \int_{b_j}^{a_{j+1}} |e'|^2 \ = \ -\sum_{j=0}^{J} \int_{b_j}^{a_{j+1}} e'' \, e$$

$$= \ \sum_{j=0}^{J} \int_{b_j}^{a_{j+1}} (f - \Pi_H f) \, e. \tag{6}$$

Note that the integration by parts here does not give rise to any boundary or jump terms because e vanishes at all the points a_j, b_j and also at the grid points x_i where e' is discontinuous. We now apply the Cauchy-Schwarz and Poincaré inequalities on each segment (b_j, a_{j+1}) and note that the constant in the latter inequality scales as the length of the segment, that is at most ε

(this fact is obvious in dimension $d = 1$; see (23) and Appendix A.1 below for a general argument). We thus deduce from (6) that

$$
\begin{aligned}
|e|^2_{H^1(\Omega_\varepsilon)} &\leq \sum_{j=0}^{J} \|f - \Pi_H f\|_{L^2(b_j, a_{j+1})} \, \|e\|_{L^2(b_j, a_{j+1})} \\
&\leq C\varepsilon \sum_{j=0}^{J} \|f - \Pi_H f\|_{L^2(b_j, a_{j+1})} \, |e|_{H^1(b_j, a_{j+1})} \\
&\leq C\varepsilon \|f - \Pi_H f\|_{L^2(\Omega_\varepsilon)} \, |e|_{H^1(\Omega_\varepsilon)}.
\end{aligned}
$$

Factoring out $|e|_{H^1(\Omega_\varepsilon)}$, and using a standard finite element approximation estimate of $f - \Pi_H f$, we deduce that

$$
|u - v_H|_{H^1(\Omega_\varepsilon)} = |e|_{H^1(\Omega_\varepsilon)} \leq C\varepsilon \|f - \Pi_H f\|_{L^2(\Omega)} \leq C\varepsilon H \|f'\|_{L^2(\Omega)}.
$$

Collecting this bound with (5), we obtain (4). $\qquad\square$

2 Presentation of our MsFEM approach in the 2D setting

2.1 MsFEM à la Crouzeix-Raviart with bubble functions

As mentioned in the introduction, we assume henceforth that the ambient dimension is $d = 2$ and that Ω is a polygonal domain. We define a mesh $\mathcal{T}_H$ on Ω, i.e. a decomposition of Ω into polygons each of diameter at most H, and denote $\mathcal{E}_H$ the set of all the internal edges of $\mathcal{T}_H$. Note that we mesh Ω and not the perforated domain Ω_ε. This allows us to use coarse elements (independently of the fine scale present in the geometry of Ω_ε), and leaves us with a lot of flexibility. The mesh does not have to be consistent with the perforations B_ε. Some nodes may be in B_ε, and likewise some edges may intersect B_ε.

We also assume that the mesh does not have any hanging nodes. Otherwise stated, each internal edge is shared by exactly two elements of the mesh. In addition, $\mathcal{T}_H$ is assumed a regular mesh in the following sense: for any mesh element $T \in \mathcal{T}_H$, there exists a smooth one-to-one and onto mapping

9

$K : \overline{T} \to T$ where $\overline{T} \subset \mathbb{R}^d$ is the reference element (a polygon of fixed unit diameter) and $\|\nabla K\|_{L^\infty} \leq CH$, $\|\nabla K^{-1}\|_{L^\infty} \leq CH^{-1}$, C being some universal constant independent of T, to which we will refer as the regularity parameter of the mesh. This assumption is used e.g. in the proof of Lemma 9 below. To avoid some technical complications, we also assume that the mapping K corresponding to each $T \in \mathcal{T}_H$ is affine on every edge of $\partial \overline{T}$. Again, this assumption is used e.g. in the proof of Lemma 9. In the following and to fix the ideas, we will have in mind a mesh consisting of *triangles*, which satisfies the minimum angle condition to ensure the mesh is regular in the sense defined above (see e.g. [4, Section 4.4]). We will repeatedly use the notation and terminology (triangle, . . .) of this setting, although the approach carries over to quadrangles.

The idea behind the MsFEM à la Crouzeix-Raviart is to require the continuity of the (here highly oscillatory) finite element functions in the sense of averages on the edges. We have extensively studied this approach in [21]. For the specific setting we address here, we add another feature to the numerical approach. Based in particular on the intuition provided by the one-dimensional case examined in the previous section, we add *bubble functions* to our discretization space.

Functional spaces To construct our MsFEM space, we proceed as in our previous work [21]. We introduce the space

$$
W_H = \left\{ \begin{array}{l} u \in L^2(\Omega) \text{ such that } u|_T \in H^1(T) \text{ for any } T \in \mathcal{T}_H, \\ \displaystyle\int_E [[u]] = 0 \text{ for all } E \in \mathcal{E}_H, \quad u = 0 \text{ in } B_\varepsilon \text{ and on } \partial\Omega \end{array} \right\},
$$

where $[[u]]$ denotes the jump of u across an edge. Note that, as is standard, the condition $u = 0$ on $\partial\Omega$ makes sense as Ω is a polygonal domain and $\partial\Omega$ belongs to the mesh edges. We next introduce the subspace

$$
W_H^0 = \left\{ \begin{array}{l} u \in W_H \text{ such that } \displaystyle\int_E u = 0 \text{ for all } E \in \mathcal{E}_H \\ \text{and } \displaystyle\int_T u = 0 \text{ for all } T \in \mathcal{T}_H \end{array} \right\}
$$

of W_H and define the MsFEM space à la Crouzeix-Raviart

$$
V_H = \left\{ u \in W_H \text{ such that } a_H(u,v) = 0 \text{ for all } v \in W_H^0 \right\} \tag{7}
$$

as the orthogonal complement of W_H^0 in W_H, where by orthogonality we mean orthogonality for the scalar product defined by

$$a_H(u,v) := \sum_{T \in \mathcal{T}_H} \int_{T \cap \Omega_\varepsilon} \nabla u \cdot \nabla v. \tag{8}$$

We use a broken integral in the definition of a_H since $W_H \not\subset H^1(\Omega)$.

Notation For any $u \in V_H + H_0^1(\Omega_\varepsilon)$, we denote by

$$|u|_{H_H^1(\Omega_\varepsilon)} := \sqrt{a_H(u,u)} \tag{9}$$

the energy norm associated with the form a_H.

Likewise, for any $u \in H_0^1(\Omega_\varepsilon)$, we denote by

$$|u|_{H^1(\Omega_\varepsilon)} := \sqrt{\int_{\Omega_\varepsilon} |\nabla u|^2}$$

the H^1 semi-norm.

Strong form and basis functions of V_H Consider any element $T \in \mathcal{T}_H$ (the three edges of which are denoted Γ_i, $1 \le i \le 3$). Taking in the definition of V_H a function v that vanishes on $\Omega \setminus T$, we note that any function $u \in V_H$ satisfies

$$\int_{T \cap \Omega_\varepsilon} \nabla u \cdot \nabla v = 0$$

for all $v \in H^1(T)$ such that $v = 0$ in B_ε, $\int_{\Gamma_i} v = 0$ for all i (if $\Gamma_i \subset \partial\Omega$, the condition $\int_{\Gamma_i} v = 0$ is replaced by $v = 0$ on Γ_i) and $\int_T v = 0$. This can be rewritten as

$$\int_{T \cap \Omega_\varepsilon} \nabla u \cdot \nabla v = \lambda_0^T \int_T v + \sum_{i=1}^3 \lambda_i^T \int_{\Gamma_i} v \quad \text{for all } v \in H^1(T) \text{ s.t. } v = 0 \text{ in } B_\varepsilon$$

for some scalar constants λ_j^T, $0 \le j \le 3$ (on purpose, we have made the dependence of these constants explicit with respect to the mesh element T).

11

Hence, the restriction of any $u \in V_H$ to T is in particular a solution to the boundary value problem

$$- \Delta u = \lambda_0^T \text{ in } T \setminus B_\varepsilon, \quad u = 0 \text{ in } T \cap B_\varepsilon, \quad n \cdot \nabla u = \lambda_i^T \text{ on each } \Gamma_i. \quad (10)$$

The flux along each edge interior to Ω is therefore a constant, the constant being possibly different on the two sides of the edge.

The above observation shows that V_H is a finite dimensional space. We now construct a basis for V_H, which consists of functions associated to a particular mesh element or a particular internal edge. Note that no basis function is associated to edges belonging to $\partial\Omega$.

First, for any mesh element T that is not a subset of the perforations B_ε (i.e. $T \not\subset B_\varepsilon$), we consider the variational problem

$$\inf \left\{ \begin{array}{l} \displaystyle\int_{T \setminus B_\varepsilon} \left[\frac{1}{2} |\nabla\Psi|^2 - \Psi \right], \ \Psi \in H^1(T), \\[2mm] \Psi = 0 \text{ in } T \cap B_\varepsilon, \ \displaystyle\int_{\Gamma_i} \Psi = 0 \text{ for each } \Gamma_i \end{array} \right\}. \quad (11)$$

Using the Poincaré inequality recalled in [21, Lemma 9] and standard analysis arguments, we see that this problem has a unique minimizer. We then introduce the function $\Psi_T \in L^2(\Omega)$ which vanishes in $\Omega \setminus T$ and is equal to this minimizer in T. We easily deduce from the optimality condition that $\Psi_T \in V_H$ and satisfies

$$-\Delta\Psi_T = 1 \text{ in } T \setminus B_\varepsilon, \quad \Psi_T = 0 \text{ in } T \cap B_\varepsilon,$$

with, for each edge Γ_i of T, $\displaystyle\int_{\Gamma_i} \Psi_T = 0$ and $n \cdot \nabla\Psi_T = \lambda_i$ on Γ_i for some constant λ_i.

Second, for any internal edge E that is not a subset of the perforations B_ε, we denote T_E^1 and T_E^2 the two triangles sharing this edge, set $T_E := T_E^1 \cup T_E^2$, and consider the variational problem

$$\inf \left\{ \begin{array}{l} \displaystyle\int_{T_E^1 \setminus B_\varepsilon} |\nabla\Phi|^2 + \int_{T_E^2 \setminus B_\varepsilon} |\nabla\Phi|^2, \ \Phi|_{T_E^1} \in H^1(T_E^1), \ \Phi|_{T_E^2} \in H^1(T_E^2), \\[2mm] \Phi = 0 \text{ in } T_E \cap B_\varepsilon, \ \displaystyle\int_E \Phi = 1, \ \int_{E'} \Phi = 0 \text{ for any edge } E' \subset \partial T_E \end{array} \right\}. \quad (12)$$

This set is not empty due to the fact that $E \not\subset B_\varepsilon$. Again, this problem has a unique minimizer. We introduce the function $\Phi_E \in L^2(\Omega)$ which vanishes in $\Omega \setminus T_E$ and is equal to this minimizer in T_E. We easily deduce from the optimality condition that $\Phi_E \in V_H$ and satisfies

$$-\Delta \Phi_E = 0 \text{ in } T_E^1 \setminus B_\varepsilon, \quad -\Delta \Phi_E = 0 \text{ in } T_E^2 \setminus B_\varepsilon, \quad \Phi_E = 0 \text{ in } T \cap B_\varepsilon,$$

with, for each edge $E' \subset \partial T_E$, $\displaystyle\int_{E'} \Phi_E = 0$ and $n \cdot \nabla \Phi_E = \lambda_{E'}$ on E' for some constant $\lambda_{E'}$ and $\displaystyle\int_E \Phi_E = 1$ and $n \cdot \nabla \Phi_E = \lambda_E$ on E for some constant λ_E (with an a priori different constant on the two sides of E).

For any mesh element $T \subset B_\varepsilon$ (resp. any internal edge $E \subset B_\varepsilon$), we set $\Psi_T \equiv 0$ (resp. $\Phi_E \equiv 0$).

Remark 3. *In the one-dimensional case, the functions Ψ_T and Φ_E that we have defined are equal to the basis functions of Section 1.2 (see Figures 2 and 3).*

The functions Ψ_T and Φ_E that we have constructed belong to V_H. In addition, $\{\Psi_T\}_{T \in \mathcal{T}_H, \, T \not\subset B_\varepsilon} \cup \{\Phi_E\}_{E \in \mathcal{E}_H, \, E \not\subset B_\varepsilon}$ forms a linearly independent family. We have

$$\text{Span} \{\Phi_E, \Psi_T, \, E \in \mathcal{E}_H, \, T \in \mathcal{T}_H\} \subset V_H.$$

Conversely, let $u \in V_H$. We know that u satisfies (10). We introduce

$$v = u - \sum_{T \in \mathcal{T}_H} \lambda_0^T \Psi_T - \sum_{E \in \mathcal{E}_H} \left[\int_E u \right] \Phi_E$$

and note that it satisfies, for any $T \in \mathcal{T}_H$,

$$-\Delta v = 0 \text{ in } T \setminus B_\varepsilon, \quad v = 0 \text{ in } T \cap B_\varepsilon,$$

with $\displaystyle\int_E v = 0$ and $n \cdot \nabla v$ is a constant on E, for each edge $E \in \mathcal{E}_H$. This implies that $v \equiv 0$, and thus

$$V_H = \text{Span} \{\Phi_E, \Psi_T, \, E \in \mathcal{E}_H, \, T \in \mathcal{T}_H\}. \tag{13}$$

13

Numerical approximation The MsFEM approximate solution of our problem (1) is defined as the solution $u_H \in V_H$ to

$$\forall v_H \in V_H, \quad a_H(u_H, v_H) = \int_{\Omega_\varepsilon} f v_H, \tag{14}$$

where a_H is defined by (8).

2.2 Main result: an error estimate in the case of periodic perforations

The main theoretical result we obtain in this article addresses the numerical analysis of the approach presented above, in the particular case of periodic perforations in dimension 2, with a sufficient regularity (made precise in the statement of the theorem below) of the right-hand side f of (1).

Theorem 4. *Let u be the solution to (1) for $d = 2$, with periodic perforations and with $f \in H^2(\Omega)$. We assume that, loosely speaking, the slopes of the mesh edges are rational numbers. More precisely, we assume that the equation of any internal edge E of the mesh writes $x_2 = \dfrac{p_E}{q_E} x_1 + c_E$ for some $c_E \in \mathbb{R}$, some $p_E \in \mathbb{Z}$ and $q_E \in \mathbb{N}^\star$ that are coprime, with*

$$|q_E| \leq C \tag{15}$$

for a constant C independent of the edge considered in the mesh and of the mesh size H.

Then the MsFEM approximation u_H, solution to (14), satisfies

$$|u - u_H|_{H^1_H(\Omega_\varepsilon)} \leq C\varepsilon \left(\sqrt{\varepsilon} + H + \sqrt{\frac{\varepsilon}{H}} \right) \|f\|_{H^2(\Omega)}, \tag{16}$$

for some universal constant C independent from H, ε and f, but depending on the geometry of the mesh and other parameters of the problem.

As will be evident from the theoretical ingredients recalled below (see (18) and comments following this estimate), the right-hand side of (16) needs to be understood as follows. The size of the exact solution u (and thus that of the corresponding approximation u_H) is ε in H^1 norm. Taking this scale factor into account, the actual rate of convergence for the numerical approach we design is therefore given by $\sqrt{\varepsilon} + H + \sqrt{\varepsilon/H}$.

Remark 5. *Our assumption on the rationality of the slopes in the mesh is necessary, in the current state of our understanding, to treat traces of periodic functions on the edges of the mesh. In full generality, such traces are almost periodic functions. Our proof perhaps carries over to this case, however at the price of unnecessary technicalities (we refer e.g. to [13, 14] for works on boundary layers in homogenization, where such non-periodic situations are dealt with). In the case of rational slopes we restrict ourselves to, these traces are periodic, and the uniform bound (15) we additionally assume enables us to uniformly bound their periods from above, rending the proof much easier. We emphasize that our assumption does not seem to us very restrictive in practice.*

Remark 6. *It is useful to compare our error estimate (16) with estimates for other existing MsFEM-type approaches established for similar problems. First, we are not aware of any other numerical analysis of a MsFEM-type approach for problems set on perforated domains. To the best of our knowledge, this work is the first one proposing and analyzing a MsFEM-type approach specifically adapted to such problems.*

Second, as pointed out above, this work is a follow up on our previous work [21] where we have studied a Crouzeix-Raviart type MsFEM approach on the problem

$$-\operatorname{div}\left[A_\varepsilon(x)\nabla u^\varepsilon\right] = f \ \text{in } \Omega, \quad u^\varepsilon = 0 \ \text{on } \partial\Omega, \tag{17}$$

the main difference between that method and the one presented here being the addition of bubble functions in the MsFEM space. For problem (17), we have compared in [21, Remark 3.2] our error estimate with those obtained for other MsFEM-type approaches.

Remark 7. *In the absence of perforations, our problem simply writes*

$$-\Delta u = f \ \text{in } \Omega, \quad u = 0 \ \text{on } \partial\Omega.$$

Assuming a triangular mesh is used, our discretization space V_H then becomes the standard Crouzeix-Raviart space [9] (see [21, Remark 1.1]), complemented by bubble functions defined by (11) with $B_\varepsilon = \emptyset$. In turn, the MsFEM approach with linear boundary conditions (as well as the oversampling variant) then becomes the standard P1 FEM.

The next two sections are devoted to the proof of Theorem 4. Numerical results are gathered in Section 5.

3 Some preliminaries

3.1 Elements of homogenization theory for periodically perforated domains

We consider the unit square Y and some smooth perforation $B \subset Y$. We next scale B and Y by a factor ε and then periodically repeat this pattern with periods ε in both directions. The set of perforations is therefore

$$B_\varepsilon = \Omega \cap \left(\underset{k \in \mathbb{Z}^2}{\cup} \varepsilon B_k \right) \quad \text{with} \quad B_k = k + B$$

and the perforated domain is $\Omega_\varepsilon = \Omega \setminus \overline{B_\varepsilon}$. We denote by u^ε the solution to (1) to emphasize the dependency upon ε. We know from the classical work [22] that, provided f vanishes on the boundary of Ω (see below the easy adaptation to a more general case), we have

$$\left| u^\varepsilon - \varepsilon^2 w \left(\frac{\cdot}{\varepsilon} \right) f \right|_{H^1(\Omega_\varepsilon)} \le C\varepsilon^2 \|f\|_{H^2(\Omega)}, \tag{18}$$

where w denotes the corrector, that is the solution to the problem

$$\begin{aligned} -\Delta w &= 1 \text{ on } Y \setminus B, \\ w &= 0 \text{ on } \overline{B}, \\ & w \text{ is } Y\text{-periodic}, \end{aligned} \tag{19}$$

in the unit cell Y. We refer to [3, 11, 20] for more background on homogenization theory. Note that (18) is *not* restricted to the two-dimensional case. In the sequel, we will use the fact that

$$w \in C^1 \left(\overline{Y \setminus B} \right), \tag{20}$$

which follows from the fact that $w \in C^{2,\delta} \left(\overline{Y \setminus B} \right)$ for some $\delta > 0$ (see e.g. [15, Theorem 6.14]). In view of [15, Corollary 8.11], we also have $w \in C^\infty(Y \setminus B)$, but we will not need this henceforth.

Clearly, (18) shows that, for ε small, the dominant behaviour of the solution u^ε to (1) is simple. It is obtained by a simple multiplication of the right-hand side f by the corrector function. Otherwise stated, the particular

setting yields an homogenized problem where the differential operator has disappeared. The corrector problem (19) formally agrees with intuition: at the scale of the geometric heterogeneities, the right-hand side f of (1) is seen as a constant function (thus the right-hand side of (19)) and the approximation of the solution u^ε is obtained by the simple multiplication mentioned above. Additionally, the "size" of the solution u^ε is proportional to ε^2 in L^2 norm and ε in H^1 norm, a fact that will need to be borne in mind below when performing the analysis and the numerical experiments.

It is easy to modify (18) in order to accomodate the more general situation where the right-hand side $f \in H^2(\Omega)$ does not necessarily vanish on the boundary of Ω, provided the domain Ω is smooth. We then have the weaker estimate

$$\left| u^\varepsilon - \varepsilon^2 w\left(\frac{\cdot}{\varepsilon}\right) f \right|_{H^1(\Omega_\varepsilon)} \leq C\varepsilon^{3/2} \mathcal{N}(f), \tag{21}$$

where

$$\mathcal{N}(f) = \|f\|_{L^\infty(\Omega)} + \|\nabla f\|_{L^2(\Omega)} + \|\Delta f\|_{L^2(\Omega)}. \tag{22}$$

We recall that, in dimension $d = 2$, the injection $H^2(\Omega) \subset C^0(\overline{\Omega})$ is continuous. The proof of (21) is postponed until Appendix A.2.

A key ingredient for that proof, and for other proofs throughout this article, is the following Poincaré inequality in the perforated domain Ω_ε: there exists a constant C independent of ε such that

$$\forall \phi \in H^1_0(\Omega_\varepsilon), \quad \|\phi\|_{L^2(\Omega_\varepsilon)} \leq C\varepsilon \|\nabla \phi\|_{L^2(\Omega_\varepsilon)} = C\varepsilon |\phi|_{H^1(\Omega_\varepsilon)}. \tag{23}$$

The proof of (23) is postponed until Appendix A.1. Following the same arguments, we also see that there exists a constant C independent of ε such that

$$\forall \phi \in W_H, \quad \|\phi\|_{L^2(\Omega_\varepsilon)} \leq C\varepsilon |\phi|_{H^1_H(\Omega_\varepsilon)}, \tag{24}$$

where, we recall, the notation $|\cdot|_{H^1_H(\Omega_\varepsilon)}$ has been defined in (9). The condition $\int_E [[\phi]] = 0$ (present in the definition of W_H) is actually not needed for (24) to hold, given that $\phi = 0$ on B_ε.

3.2 Classical ingredients of multiscale numerical analysis

Before we get to the proof of Theorem 4, we first need to collect here some standard Trace theorems (which were already used and proved in [21]) and

17

results on the convergence of oscillating functions. We refer to the textbooks [4, 12, 15] for more details. Remark that only Lemma 11 is restricted to the two-dimensional setting.

First we recall the definition, borrowed from e.g. [12, Definition B.30], of the $H^{1/2}$ space.

Definition 8. *For any open domain $\omega \subset \mathbb{R}^n$, we define the norm*

$$\|u\|^2_{H^{1/2}(\omega)} := \|u\|^2_{L^2(\omega)} + |u|^2_{H^{1/2}(\omega)},$$

where

$$|u|^2_{H^{1/2}(\omega)} := \int_\omega \int_\omega \frac{|u(x) - u(y)|^2}{|x - y|^{n+1}}\, dxdy,$$

and define the space

$$H^{1/2}(\omega) := \left\{ u \in L^2(\omega), \quad \|u\|_{H^{1/2}(\omega)} < \infty \right\}.$$

Trace inequalities   We have the following trace results:

Lemma 9. *There exists C (depending only on the regularity of the mesh) such that, for any $T \in \mathcal{T}_H$ and any edge $E \subset \partial T$, we have*

$$\forall v \in H^1(T), \quad \|v\|^2_{L^2(E)} \leq C \left(H^{-1} \|v\|^2_{L^2(T)} + H \|\nabla v\|^2_{L^2(T)} \right). \tag{25}$$

Under the additional assumption that $\int_E v = 0$, we have

$$\|v\|^2_{L^2(E)} \leq CH \|\nabla v\|^2_{L^2(T)} \tag{26}$$

and

$$\|v\|^2_{H^{1/2}(E)} \leq C(1 + H) \|\nabla v\|^2_{L^2(T)}. \tag{27}$$

These bounds are classical results (see e.g. [4, page 282]) and are proved in [21, Section 4.2]. The following result is a direct consequence of (26) and (27):

Corollary 10. *Consider an edge $E \in \mathcal{E}_H$, and let $T_E \subset \mathcal{T}_H$ denote all the triangles sharing this edge. There exists C (depending only on the regularity of the mesh) such that*

$$\forall v \in W_H, \quad \| [[v]] \|^2_{L^2(E)} \leq CH \sum_{T \in T_E} \|\nabla v\|^2_{L^2(T)} \tag{28}$$

18

and

$$\forall v \in W_H, \quad \| \, [[v]] \, \|^2_{H^{1/2}(E)} \leq C(1+H) \sum_{T \in T_E} \|\nabla v\|^2_{L^2(T)}. \qquad (29)$$

Averages of oscillatory functions   We shall also need the following classical result.

Lemma 11. *Let $g \in L^\infty(\mathbb{R})$ be a q-periodic function with zero mean. Let $f \in W^{1,1}(0,H) \subset C^0(0,H)$ be a function defined on the interval $[0,H]$ that vanishes at least at one point of $[0,H]$. Then, for any $\varepsilon > 0$,*

$$\left| \int_0^H g\left(\frac{x}{\varepsilon}\right) f(x) dx \right| \leq 2\varepsilon q \|g\|_{L^\infty(\mathbb{R})} \|f'\|_{L^1(0,H)}.$$

Proof. The proof is simple and essentially based upon an integration by parts. Let G be a primitive of g:

$$G(x) = \int_0^x g(t) dt.$$

The function G is q-periodic (as the average of g over its period vanishes) and bounded, with $\|G\|_{L^\infty(\mathbb{R})} \leq q\|g\|_{L^\infty(\mathbb{R})}$. Supposing that the function f vanishes at the point $c \in [0,H]$, we write

$$\begin{aligned}
\int_c^H g\left(\frac{x}{\varepsilon}\right) f(x) \, dx &= \int_c^H G'\left(\frac{x}{\varepsilon}\right) f(x) \, dx \\
&= \varepsilon G\left(\frac{H}{\varepsilon}\right) f(H) - \int_c^H \varepsilon G\left(\frac{x}{\varepsilon}\right) f'(x) \, dx \\
&= \varepsilon G\left(\frac{H}{\varepsilon}\right) \int_c^H f'(x) \, dx - \int_c^H \varepsilon G\left(\frac{x}{\varepsilon}\right) f'(x) \, dx,
\end{aligned}$$

hence

$$\left| \int_c^H g\left(\frac{x}{\varepsilon}\right) f(x) \, dx \right| \leq 2\varepsilon \|G\|_{L^\infty(\mathbb{R})} \|f'\|_{L^1(c,H)} \leq 2\varepsilon q \|g\|_{L^\infty(\mathbb{R})} \|f'\|_{L^1(c,H)}.$$

By a similar computation,

$$\left| \int_0^c g\left(\frac{x}{\varepsilon}\right) f(x) \, dx \right| \leq 2\varepsilon q \|g\|_{L^\infty(\mathbb{R})} \|f'\|_{L^1(0,c)}.$$

The above two bounds imply the result. $\qquad\square$

4 Proof of our main result

To prove Theorem 4, it is possible to follow the same arguments as in our earlier work [21]. We follow here a different path, so as to show that other strategies are possible. Note that we use here and in [21] the same technical ingredients, including those recalled in Section 3.2 and an interpolation argument, see Step 1c below.

Let u be the solution to the reference problem (1) with the right-hand side f, and let $\Pi_H f$ be the L^2-orthogonal projection of f on the space of piecewise constant functions. We recall the following standard finite element interpolation result: there exists C independent of H and f such that

$$\|f - \Pi_H f\|_{L^2(\Omega)} \leq CH \|\nabla f\|_{L^2(\Omega)}. \tag{30}$$

We introduce

$$v_H(x) = \sum_{T \in \mathcal{T}_H} \Pi_H f \ \Psi_T(x) + \sum_{E \in \mathcal{E}_H} \left[\int_E u \right] \Phi_E(x), \tag{31}$$

where the functions Ψ_T and Φ_E have been defined in Section 2.1 by (11) and (12) respectively. We recall that, if $T \subset B_\varepsilon$ (resp. $E \subset B_\varepsilon$), then $\Psi_T \equiv 0$ (resp. $\Phi_E \equiv 0$). We see from (13) that $v_H \in V_H$. We next decompose the exact solution u of (1) in the form

$$u = v_H + \phi.$$

By definition of Ψ_T and Φ_E, we have, for all edges $E \in \mathcal{E}_H$ and all triangles $T \in \mathcal{T}_H$, that

$$\begin{aligned} \int_E v_H &= \int_E u \quad \text{hence} \quad \int_E \phi = 0, \\ n \cdot \nabla v_H &= \text{Constant on (each side of) } E, \\ -\Delta v_H &= \Pi_H f \text{ on } T \cap \Omega_\varepsilon. \end{aligned} \tag{32}$$

The estimate (16) is proved by estimating $\phi = u - v_H$ in Step 1 below and next $v_H - u_H$ in Step 2.

In what follows, we use the shorthand notation $g_\varepsilon(x) = g(x/\varepsilon)$ for all functions g. The notation C stands for a constant that is independent from ε, H, f and u, and that may vary from one line to the next.

Step 1: Estimation of $u - v_H$: Using the approximation of u given by the homogenization result (21), we write

$$
\begin{aligned}
|\phi|^2_{H^1_H(\Omega_\varepsilon)} &= \sum_{T \in \mathcal{T}_H} \int_{\Omega_\varepsilon \cap T} |\nabla \phi|^2 \\
&= \sum_{T \in \mathcal{T}_H} \int_{\Omega_\varepsilon \cap T} \nabla(u - \varepsilon^2 w_\varepsilon f) \cdot \nabla\phi + \sum_{T \in \mathcal{T}_H} \int_{\Omega_\varepsilon \cap T} \nabla(\varepsilon^2 w_\varepsilon f - v_H) \cdot \nabla\phi \\
&= \sum_{T \in \mathcal{T}_H} \int_{\Omega_\varepsilon \cap T} \nabla(u - \varepsilon^2 w_\varepsilon f) \cdot \nabla\phi + \sum_{T \in \mathcal{T}_H} \int_{\Omega_\varepsilon \cap T} (-\Delta(\varepsilon^2 w_\varepsilon f - v_H))\phi \\
&\quad + \varepsilon^2 \sum_{T \in \mathcal{T}_H} \int_{\partial(T \cap \Omega_\varepsilon)} \phi \, n \cdot \nabla(w_\varepsilon f) - \sum_{T \in \mathcal{T}_H} \int_{\partial(T \cap \Omega_\varepsilon)} \phi \, n \cdot \nabla v_H. \quad (33)
\end{aligned}
$$

We now use the fact that $\phi = u - v_H = 0$ on $\partial\Omega_\varepsilon$. We hence have that

$$
\int_{\partial(T \cap \Omega_\varepsilon)} \phi \, n \cdot \nabla(w_\varepsilon f) = \int_{(\partial T) \cap \Omega_\varepsilon} \phi \, n \cdot \nabla(w_\varepsilon f) \qquad (34)
$$

and likewise for the last term of (33). Equalities of the type (34) will often be used in the sequel. We thus write (33) as

$$
\begin{aligned}
|\phi|^2_{H^1_H(\Omega_\varepsilon)} &= \sum_{T \in \mathcal{T}_H} \int_{\Omega_\varepsilon \cap T} \nabla(u - \varepsilon^2 w_\varepsilon f) \cdot \nabla\phi + \sum_{T \in \mathcal{T}_H} \int_{\Omega_\varepsilon \cap T} (-\Delta(\varepsilon^2 w_\varepsilon f - v_H))\phi \\
&\quad + \varepsilon^2 \sum_{T \in \mathcal{T}_H} \int_{(\partial T) \cap \Omega_\varepsilon} \phi \, n \cdot \nabla(w_\varepsilon f) - \sum_{T \in \mathcal{T}_H} \int_{(\partial T) \cap \Omega_\varepsilon} \phi \, n \cdot \nabla v_H.
\end{aligned}
$$

The fourth term in the above right-hand side vanishes. Indeed, on each edge E, we know from (32) that $n \cdot \nabla v_H$ is constant and $\int_E \phi = \int_{E \cap \Omega_\varepsilon} \phi = 0$. The third term can be written

$$
\varepsilon^2 \sum_{T \in \mathcal{T}_H} \int_{(\partial T) \cap \Omega_\varepsilon} \phi \, n \cdot \nabla(w_\varepsilon f) = \varepsilon^2 \sum_{E \in \mathcal{E}_H} \int_{E \cap \Omega_\varepsilon} [[\phi]] \, n \cdot \nabla(w_\varepsilon f).
$$

Indeed, $w \in C^1\left(\overline{Y \setminus B}\right)$ (see (20)) and $f \in H^2(\Omega)$, hence $\nabla(w_\varepsilon f)$ has a well-defined trace on $E \cap \Omega_\varepsilon$. We are thus left with

$$
\begin{aligned}
|\phi|^2_{H^1_H(\Omega_\varepsilon)} &= \sum_{T \in \mathcal{T}_H} \int_{\Omega_\varepsilon \cap T} \nabla(u - \varepsilon^2 w_\varepsilon f) \cdot \nabla\phi + \sum_{T \in \mathcal{T}_H} \int_{\Omega_\varepsilon \cap T} (-\Delta(\varepsilon^2 w_\varepsilon f - v_H))\phi \\
&\quad + \varepsilon^2 \sum_{E \in \mathcal{E}_H} \int_{E \cap \Omega_\varepsilon} [[\phi]] \, n \cdot \nabla(w_\varepsilon f). \qquad (35)
\end{aligned}
$$

21

We now successively bound the three terms of the right-hand side of (35). Loosely speaking:

- the first term is small because of the homogenization result (21), that states that $\varepsilon^2 w_\varepsilon f$ is indeed an accurate approximation of u.

- the second term is small because, at the leading order term in ε, the first factor in the integrand is equal to $-\Delta\left(\varepsilon^2 w_\varepsilon f\right) + \Delta v_H \approx f - \Pi_H f$ which is small due to (30).

- estimating the third term is more involved. An essential ingredient is the fact that w is a periodic function. We are thus in position to apply our Lemma 11.

Step 1a The first term of (35) is easily estimated as follows:

$$
\begin{aligned}
\left| \sum_{T \in \mathcal{T}_H} \int_{\Omega_\varepsilon \cap T} \nabla(u - \varepsilon^2 w_\varepsilon f) \cdot \nabla \phi \right| &\leq \sum_{T \in \mathcal{T}_H} \|\nabla(u - \varepsilon^2 w_\varepsilon f)\|_{L^2(\Omega_\varepsilon \cap T)} \|\nabla \phi\|_{L^2(\Omega_\varepsilon \cap T)} \\
&\leq |u - \varepsilon^2 w_\varepsilon f|_{H^1(\Omega_\varepsilon)} \, |\phi|_{H^1_H(\Omega_\varepsilon)} \\
&\leq C \varepsilon^{3/2} \mathcal{N}(f) \, |\phi|_{H^1_H(\Omega_\varepsilon)},
\end{aligned}
\tag{36}
$$

where we have used the discrete Cauchy-Schwarz inequality in the second line and the homogenization result (21) in the third line.

Step 1b We next turn to the second term of the right-hand side of (35), that we write as follows, using the corrector equation (19) and (32):

$$
\sum_{T \in \mathcal{T}_H} \int_{\Omega_\varepsilon \cap T} (-\Delta(\varepsilon^2 w_\varepsilon f - v_H))\phi = \int_{\Omega_\varepsilon} (f - 2\varepsilon(\nabla w)_\varepsilon \cdot \nabla f - \varepsilon^2 w_\varepsilon \Delta f - \Pi_H f)\phi.
$$

We thus obtain

$$
\begin{aligned}
&\left| \sum_{T \in \mathcal{T}_H} \int_{\Omega_\varepsilon \cap T} (-\Delta(\varepsilon^2 w_\varepsilon f - v_H))\phi \right| \\
&\leq \left(\|f - \Pi_H f\|_{L^2(\Omega)} + 2\varepsilon \|\nabla w\|_{L^\infty} \|\nabla f\|_{L^2(\Omega)} + \varepsilon^2 \|w\|_{L^\infty} \|\Delta f\|_{L^2(\Omega)} \right) \|\phi\|_{L^2(\Omega_\varepsilon)} \\
&\leq C\varepsilon \left(CH \|\nabla f\|_{L^2(\Omega)} + C\varepsilon \mathcal{N}(f) \right) |\phi|_{H^1_H(\Omega_\varepsilon)},
\end{aligned}
$$

22

where $\mathcal{N}(f)$ is defined by (22) and where, in the last line, we have used (30), (20) and (24). We deduce that

$$\left| \sum_{T \in \mathcal{T}_H} \int_{\Omega_\varepsilon \cap T} (-\Delta(\varepsilon^2 w_\varepsilon f - v_H))\phi \right| \leq C\varepsilon \, (H + \varepsilon) \, \mathcal{N}(f) \, |\phi|_{H_H^1(\Omega_\varepsilon)}. \qquad (37)$$

Step 1c The final stage of Step 1 is devoted to bounding the third term of the right-hand side of (35).

In view of the assumptions on the mesh (rationality of the slopes, in short), we first observe that, for any edge $E \in \mathcal{E}_H$, the function $x \in E \mapsto n \cdot \nabla w \left(\dfrac{x}{\varepsilon} \right)$ is periodic with period $q_E \varepsilon$, for some $q_E \in \mathbb{N}^\star$ satisfying $|q_E| \leq C$ for some C independent of the mesh edge and of H. We denote by $\langle n \cdot (\nabla w)_\varepsilon \rangle_E$ the average of that function over one period, and decompose the third term of the right-hand side of (35) as follows:

$$\varepsilon^2 \sum_{E \in \mathcal{E}_H} \int_{E \cap \Omega_\varepsilon} [[\phi]] \; n \cdot \nabla (w_\varepsilon f)$$

$$= \; \varepsilon \sum_{E \in \mathcal{E}_H} \int_{E \cap \Omega_\varepsilon} [[\phi]] \; \left(n \cdot (\nabla w)_\varepsilon - \langle n \cdot (\nabla w)_\varepsilon \rangle_E \right) f$$

$$+ \; \varepsilon \sum_{E \in \mathcal{E}_H} \langle n \cdot (\nabla w)_\varepsilon \rangle_E \int_{E \cap \Omega_\varepsilon} [[\phi]] \; f + \varepsilon^2 \sum_{E \in \mathcal{E}_H} \int_{E \cap \Omega_\varepsilon} [[\phi]] \; w_\varepsilon \; n \cdot \nabla f. (38)$$

We successively estimate the three terms of the right-hand side of (38). In some formulae below, we will make the following slight abuse of notation. We will extend the function $\phi = u - v_H$ by 0 inside the perforations B_ε, so that we can understand ϕ either as a function in $H_0^1(\Omega_\varepsilon)$ or in $H_0^1(\Omega)$.

We consider the first term of the right-hand side of (38), which we evaluate essentially using the fact that it contains a periodic oscillatory function of zero mean. We claim that

$$\left| \int_{E \cap \Omega_\varepsilon} [[\phi]] \; \left(n \cdot (\nabla w)_\varepsilon - \langle n \cdot (\nabla w)_\varepsilon \rangle_E \right) f \right|$$

$$\leq C \sqrt{\varepsilon} \, \|f\|_{H^1(E)} \| \, [[\phi]] \, \|_{H^{1/2}(E)} \quad (39)$$

for a constant C independent of the edge E, ε and H. Indeed, we first note that u and v_H vanish on $\Omega \setminus \Omega_\varepsilon$, so $\phi = u - v_H$ vanishes on $E \cap (\Omega \setminus \Omega_\varepsilon)$,

hence

$$\int_{E\cap\Omega_\varepsilon} [[\phi]] \left(n\cdot(\nabla w)_\varepsilon - \langle n\cdot(\nabla w)_\varepsilon\rangle_E\right) f$$

$$= \int_E [[\phi]] \left(n\cdot(\nabla w)_\varepsilon - \langle n\cdot(\nabla w)_\varepsilon\rangle_E\right) f. \quad (40)$$

Second, using the regularity (20) of w, we obviously have that

$$\left|\int_E [[\phi]] \left(n\cdot(\nabla w)_\varepsilon - \langle n\cdot(\nabla w)_\varepsilon\rangle_E\right) f\right| \leq C \|f\|_{L^2(E)} \|\,[[\phi]]\,\|_{L^2(E)}. \quad (41)$$

Third, suppose momentarily that $[[\phi]] \in H^1(E) \subset C^0(E)$. We infer from the fact that $\int_E [[\phi]] = 0$ that $[[\phi]]$, and hence $[[\phi]]\,f$, vanishes at least at one point on E. In addition, the function $n\cdot(\nabla w)_\varepsilon - \langle n\cdot(\nabla w)_\varepsilon\rangle_E$ is periodic on E (with a period q_E uniformly bounded with respect to $E \in \mathcal{E}_H$) and of zero mean. We are then in position to apply Lemma 11, which yields, using (20),

$$\left|\int_E [[\phi]] \left(n\cdot(\nabla w)_\varepsilon - \langle n\cdot(\nabla w)_\varepsilon\rangle_E\right) f\right| \leq 4\,\varepsilon\,q_E \|\nabla w\|_{C^0} \|\nabla_E\left(f[[\phi]]\right)\|_{L^1(E)}$$

$$\leq C\,\varepsilon\,\|f\|_{H^1(E)} \|\,[[\phi]]\,\|_{H^1(E)}, \quad (42)$$

where, for any function g, $\nabla_E g = t_E \cdot \nabla g$ where t_E is a unit vector tangential to the edge E. By interpolation between (41) and (42), and using (40), we obtain (39), with a constant C (independent of the edge) which is independent from ε and H by scaling arguments (see [21] for details).

We then deduce from (39) that the first term of the right-hand side of (38)

24

satisfies

$$
\left| \varepsilon \sum_{E \in \mathcal{E}_H} \int_{E \cap \Omega_\varepsilon} [[\phi]] \left(n \cdot (\nabla w)_\varepsilon - \langle n \cdot (\nabla w)_\varepsilon \rangle_E \right) f \right|
$$

$$
\leq \quad C \, \varepsilon^{3/2} \sum_{E \in \mathcal{E}_H} \|f\|_{H^1(E)} \| [[\phi]] \|_{H^{1/2}(E)}
$$

$$
\leq \quad C \, \varepsilon^{3/2} \left(\sum_{E \in \mathcal{E}_H} \|f\|_{H^1(E)}^2 \right)^{1/2} \left(\sum_{E \in \mathcal{E}_H} \| [[\phi]] \|_{H^{1/2}(E)}^2 \right)^{1/2}
$$

$$
\leq \quad C \, \varepsilon^{3/2} \left(\sum_{E \in \mathcal{E}_H; \text{choose one } T \in T_E} \frac{1}{H}\|f\|_{H^1(T)}^2 + H\|\nabla f\|_{H^1(T)}^2 \right)^{1/2}
$$

$$
\times \left(\sum_{E \in \mathcal{E}_H} \sum_{T \in T_E} \|\nabla \phi\|_{L^2(T)}^2 \right)^{1/2},
$$

where we have used (25) of Lemma 9 and (29) of Corollary 10 (and, we recall, $T_E \subset \mathcal{T}_H$ denotes all the triangles sharing the edge E). We therefore obtain that the first term of the right-hand side of (38) satisfies

$$
\left| \varepsilon \sum_{E \in \mathcal{E}_H} \int_{E \cap \Omega_\varepsilon} [[\phi]] \left(n \cdot (\nabla w)_\varepsilon - \langle n \cdot (\nabla w)_\varepsilon \rangle_E \right) f \right|
$$

$$
\leq \quad C \, \varepsilon^{3/2} \left(\frac{1}{H}\|f\|_{H^1(\Omega)}^2 + H\|\nabla f\|_{H^1(\Omega)}^2 \right)^{1/2} |\phi|_{H_H^1(\Omega_\varepsilon)}
$$

$$
\leq \quad C \, \varepsilon \left(\sqrt{\frac{\varepsilon}{H}} \|f\|_{H^1(\Omega)} + \sqrt{\varepsilon H} \|\nabla f\|_{H^1(\Omega)} \right) |\phi|_{H_H^1(\Omega_\varepsilon)}. \qquad (43)
$$

The second term of the right-hand side of (38) has no oscillatory character. It is therefore estimated using standard arguments for Crouzeix-Raviart finite elements (using that $\int_{E \cap \Omega_\varepsilon} [[\phi]] = 0$), and the regularity of w. Introducing, for each edge E, the constant $c_E = |E|^{-1} \int_E f$, we bound the second

25

term of the right-hand side of (38) as follows:

$$
\left| \varepsilon \sum_{E \in \mathcal{E}_H} \langle n \cdot (\nabla w)_\varepsilon \rangle_E \int_{E \cap \Omega_\varepsilon} [[\phi]] \, f \right|
$$

$$
= \left| \varepsilon \sum_{E \in \mathcal{E}_H} \langle n \cdot (\nabla w)_\varepsilon \rangle_E \int_{E \cap \Omega_\varepsilon} [[\phi]] \, (f - c_E) \right|
$$

$$
\leq C\varepsilon \sum_{E \in \mathcal{E}_H} \| [[\phi]] \|_{L^2(E)} \| f - c_E \|_{L^2(E)}
$$

$$
\leq C\varepsilon \left(\sum_{E \in \mathcal{E}_H} \| [[\phi]] \|^2_{L^2(E)} \right)^{1/2} \left(\sum_{E \in \mathcal{E}_H} \| f - c_E \|^2_{L^2(E)} \right)^{1/2}
$$

$$
\leq C\varepsilon \left(\sum_{E \in \mathcal{E}_H} H \sum_{T \in T_E} \| \nabla \phi \|^2_{L^2(T)} \right)^{1/2} \left(\sum_{E \in \mathcal{E}_H; \text{choose one } T \in T_E} H \| \nabla f \|^2_{L^2(T)} \right)^{1/2}
$$

$$
\leq C\varepsilon H |\phi|_{H^1_H(\Omega_\varepsilon)} \| \nabla f \|_{L^2(\Omega)}, \tag{44}
$$

where we have used (20), (28) of Corollary 10 and (26) of Lemma 9.

We are now left with the third term of the right-hand side of (38). This term has a prefactor ε^2 and all we have to prove is that the term itself is bounded. Using again (20), (25) of Lemma 9 and (28) of Corollary 10, we obtain

$$
\left| \varepsilon^2 \sum_{E \in \mathcal{E}_H} \int_{E \cap \Omega_\varepsilon} [[\phi]] \, w_\varepsilon \, n \cdot \nabla f \right|
$$

$$
\leq C\varepsilon^2 \sum_{E \in \mathcal{E}_H} \| \nabla f \|_{L^2(E)} \| [[\phi]] \|_{L^2(E)}
$$

$$
\leq C\varepsilon^2 \left(\sum_{E \in \mathcal{E}_H} \| \nabla f \|^2_{L^2(E)} \right)^{1/2} \left(\sum_{E \in \mathcal{E}_H} \| [[\phi]] \|^2_{L^2(E)} \right)^{1/2}
$$

$$
\leq C\varepsilon^2 \left(\frac{1}{H} \sum_{T \in \mathcal{T}_H} \| \nabla f \|^2_{H^1(T)} \right)^{1/2} \left(H \sum_{T \in \mathcal{T}_H} \| \nabla \phi \|^2_{L^2(T)} \right)^{1/2}
$$

$$
\leq C\varepsilon^2 \| \nabla f \|_{H^1(\Omega)} |\phi|_{H^1_H(\Omega_\varepsilon)}. \tag{45}
$$

Collecting (38), (43), (44) and (45), we obtain that the third term of the

26

right-hand side of (35) satisfies

$$\left| \varepsilon^2 \sum_{E \in \mathcal{E}_H} \int_{E \cap \Omega_\varepsilon} [[\phi]] \, n \cdot \nabla(w_\varepsilon f) \right| \leq C\varepsilon \left(\sqrt{\frac{\varepsilon}{H}} \, \|f\|_{H^1(\Omega)} + \sqrt{\varepsilon H} \, \|\nabla f\|_{H^1(\Omega)} \right.$$

$$\left. + H \|\nabla f\|_{L^2(\Omega)} + \varepsilon \|\nabla f\|_{H^1(\Omega)} \right) |\phi|_{H^1_H(\Omega_\varepsilon)}. \quad (46)$$

Conclusion of Step 1: Collecting (35), (36), (37) and (46), we deduce that

$$
\begin{aligned}
|u - v_H|_{H^1_H(\Omega_\varepsilon)} &= |\phi|_{H^1_H(\Omega_\varepsilon)} \\
&\leq C\varepsilon \left(\sqrt{\varepsilon} + H + \sqrt{\frac{\varepsilon}{H}} \right) \left(\|f\|_{L^\infty(\Omega)} + \|\nabla f\|_{H^1(\Omega)} \right). (47)
\end{aligned}
$$

This concludes the first step of the proof.

Step 2: Estimation of $u_H - v_H$: Denoting by $\phi_H = u_H - v_H$, where u_H is the solution to (14) and v_H is defined by (31), we observe that

$$|\phi_H|^2_{H^1_H(\Omega_\varepsilon)} = a_H(u_H - v_H, \phi_H) = a_H(u - v_H, \phi_H) + a_H(u_H - u, \phi_H), \quad (48)$$

where, we recall, a_H is defined by (8). The first term is estimated using (47). The main part of this Step is thus devoted to estimating the second term of (48).

Since $\phi_H \in V_H$, we deduce from the discrete variational formulation (14) that

$$
\begin{aligned}
&a_H(u_H - u, \phi_H) \\
&= \int_{\Omega_\varepsilon} f\phi_H - \sum_{T \in \mathcal{T}_H} \int_{T \cap \Omega_\varepsilon} \nabla u \cdot \nabla \phi_H \\
&= \int_{\Omega_\varepsilon} f\phi_H - \sum_{T \in \mathcal{T}_H} \int_{T \cap \Omega_\varepsilon} \nabla(u - \varepsilon^2 w_\varepsilon f) \cdot \nabla \phi_H - \varepsilon^2 \sum_{T \in \mathcal{T}_H} \int_{T \cap \Omega_\varepsilon} \nabla(w_\varepsilon f) \cdot \nabla \phi_H \\
&= \int_{\Omega_\varepsilon} f\phi_H - \sum_{T \in \mathcal{T}_H} \int_{T \cap \Omega_\varepsilon} \nabla(u - \varepsilon^2 w_\varepsilon f) \cdot \nabla \phi_H \\
&\quad - \varepsilon^2 \sum_{T \in \mathcal{T}_H} \int_{\partial(T \cap \Omega_\varepsilon)} \phi_H \, n \cdot \nabla(w_\varepsilon f) + \varepsilon^2 \sum_{T \in \mathcal{T}_H} \int_{T \cap \Omega_\varepsilon} \phi_H \Delta(w_\varepsilon f). \quad (49)
\end{aligned}
$$

27

Since $\phi_H = 0$ on $\partial\Omega_\varepsilon$, we can take the integral in the third term of (49) only on $(\partial T) \cap \Omega_\varepsilon$. Using (19) for the fourth term, we obtain that

$$
\begin{aligned}
&a_H(u_H - u, \phi_H) \\
&= -\sum_{T \in \mathcal{T}_H} \int_{T \cap \Omega_\varepsilon} \nabla(u - \varepsilon^2 w_\varepsilon f) \cdot \nabla\phi_H - \varepsilon^2 \sum_{T \in \mathcal{T}_H} \int_{(\partial T) \cap \Omega_\varepsilon} \phi_H \, n \cdot \nabla(w_\varepsilon f) \\
&\quad + \varepsilon \sum_{T \in \mathcal{T}_H} \int_{T \cap \Omega_\varepsilon} \phi_H \Big(2(\nabla w)_\varepsilon \cdot \nabla f + \varepsilon w_\varepsilon \Delta f \Big).
\end{aligned}
\tag{50}
$$

We now successively bound the three terms of the right-hand side of (50). The first term is estimated simply using homogenization theory, since it is not specifically related to the discretization. We write, as in (36),

$$
\left| \sum_{T \in \mathcal{T}_H} \int_{\Omega_\varepsilon \cap T} \nabla(u - \varepsilon^2 w_\varepsilon f) \cdot \nabla\phi_H \right| \leq C\varepsilon^{3/2} \mathcal{N}(f) \, |\phi_H|_{H^1_H(\Omega_\varepsilon)}.
\tag{51}
$$

For the second term of the right-hand side of (50), we use the same arguments as for the third term of (35). We have

$$
\varepsilon^2 \sum_{T \in \mathcal{T}_H} \int_{(\partial T) \cap \Omega_\varepsilon} \phi_H \, n \cdot \nabla(w_\varepsilon f) = \varepsilon^2 \sum_{E \in \mathcal{E}_H} \int_{E \cap \Omega_\varepsilon} [[\phi_H]] \, n \cdot \nabla(w_\varepsilon f),
$$

and we note that $\int_E [[\phi_H]] = 0$. We therefore can use the same arguments as in Step 1c, and obtain, similarly to (46),

$$
\begin{aligned}
&\left| \varepsilon^2 \sum_{E \in \mathcal{E}_H} \int_{E \cap \Omega_\varepsilon} [[\phi_H]] \, n \cdot \nabla(w_\varepsilon f) \right| \\
&\qquad\qquad \leq C\varepsilon \left(\sqrt{\frac{\varepsilon}{H}} \|f\|_{H^1(\Omega)} + (\varepsilon + H)\|\nabla f\|_{H^1(\Omega)} \right) |\phi_H|_{H^1_H(\Omega_\varepsilon)}.
\end{aligned}
\tag{52}
$$

We next turn to the third term of the right-hand side of (50), which is estimated using the Cauchy-Schwarz inequality, the fact that the second factor is bounded and the first factor satisfies a Poincaré inequality. Indeed, using the regularity (20) of w and the Poincaré inequality (24) satisfied by

$\phi_H \in V_H \subset W_H$, we have

$$\left| \varepsilon \sum_{T \in \mathcal{T}_H} \int_{T \cap \Omega_\varepsilon} \phi_H \Big(2(\nabla w)_\varepsilon \cdot \nabla f + \varepsilon w_\varepsilon \Delta f \Big) \right|$$

$$\leq C\varepsilon \sum_{T \in \mathcal{T}_H} \|\phi_H\|_{L^2(T \cap \Omega_\varepsilon)} \left(\|\nabla f\|_{L^2(T \cap \Omega_\varepsilon)} + \varepsilon \|\Delta f\|_{L^2(T \cap \Omega_\varepsilon)} \right)$$

$$\leq C\varepsilon \|\phi_H\|_{L^2(\Omega_\varepsilon)} \|\nabla f\|_{H^1(\Omega)}$$

$$\leq C\varepsilon^2 |\phi_H|_{H_H^1(\Omega_\varepsilon)} \|\nabla f\|_{H^1(\Omega)}. \tag{53}$$

Collecting (50), (51), (52) and (53), we deduce that

$$|a_H(u_H - u, \phi_H)|$$

$$\leq C\varepsilon \left(\sqrt{\varepsilon} + H + \sqrt{\frac{\varepsilon}{H}} \right) \left(\|f\|_{L^\infty(\Omega)} + \|\nabla f\|_{H^1(\Omega)} \right) |\phi_H|_{H_H^1(\Omega_\varepsilon)}. \tag{54}$$

Inserting (54) into (48), we have

$$|\phi_H|^2_{H_H^1(\Omega_\varepsilon)}$$

$$\leq a_H(u - v_H, \phi_H) + C\varepsilon \left(\sqrt{\varepsilon} + H + \sqrt{\frac{\varepsilon}{H}} \right) \left(\|f\|_{L^\infty(\Omega)} + \|\nabla f\|_{H^1(\Omega)} \right) |\phi_H|_{H_H^1(\Omega_\varepsilon)}$$

$$\leq |u - v_H|_{H_H^1(\Omega_\varepsilon)} |\phi_H|_{H_H^1(\Omega_\varepsilon)}$$

$$+ C\varepsilon \left(\sqrt{\varepsilon} + H + \sqrt{\frac{\varepsilon}{H}} \right) \left(\|f\|_{L^\infty(\Omega)} + \|\nabla f\|_{H^1(\Omega)} \right) |\phi_H|_{H_H^1(\Omega_\varepsilon)}.$$

Factoring out $|\phi_H|_{H_H^1(\Omega_\varepsilon)}$, and using (47), we deduce that

$$|u_H - v_H|_{H_H^1(\Omega_\varepsilon)} = |\phi_H|_{H_H^1(\Omega_\varepsilon)}$$

$$\leq C\varepsilon \left(\sqrt{\varepsilon} + H + \sqrt{\frac{\varepsilon}{H}} \right) \left(\|f\|_{L^\infty(\Omega)} + \|\nabla f\|_{H^1(\Omega)} \right) \tag{55}$$

Conclusion We deduce from (47), (55) and the triangle inequality that

$$|u - u_H|_{H_H^1(\Omega_\varepsilon)} \leq C\varepsilon \left(\sqrt{\varepsilon} + H + \sqrt{\frac{\varepsilon}{H}} \right) \left(\|f\|_{L^\infty(\Omega)} + \|\nabla f\|_{H^1(\Omega)} \right),$$

which is the desired estimate (16). This concludes the proof of Theorem 4.

5   Numerical tests

We now solve (1) for some particular settings, comparing our approach with other existing MsFEM type methods. As pointed out in the introduction, we numerically explore the influence of three parameters:

- (i) the boundary conditions imposed to define the MsFEM basis functions and (ii) the addition, or not, of bubble functions. To do so, in Section 5.1, we compare the approach we propose with other existing approaches, considering two versions of each approach, one with and the other without bubble functions.

- (iii) the possible intersections of the perforations with the edges of mesh elements. We address this question in Section 5.2, and check there the robustness of our approach with respect to the location of the perforations: the fact that the mesh intersects, or does not intersect, the perforations has a very little influence on the (good) accuracy of our approach, in contrast to other approaches.

We eventually turn in Section 5.3 to a non-periodic test-case, where we again show the excellent performance of our approach.

We mention that, in all our numerical experiments, we actually do not directly solve (1) but a penalized version of this problem: find $u \in H_0^1(\Omega)$ such that

$$- \operatorname{div}(\nu \nabla u) + \sigma u = f$$

with the following penalization parameters:

$$\nu = \left\{ \begin{array}{l} 1 \text{ in } \Omega \setminus B_\varepsilon \\ \dfrac{1}{h} \text{ in } B_\varepsilon \end{array} \right. \quad \text{and} \quad \sigma = \left\{ \begin{array}{l} 0 \text{ in } \Omega \setminus B_\varepsilon \\ \dfrac{1}{h^3} \text{ in } B_\varepsilon \end{array} \right. ,$$

where h is the fine-scale mesh size used to precompute the highly oscillatory basis functions (see [1, 5] for more details on the penalization approach and on the above choice of ν and σ). In practice, the chosen fine-scale mesh size always satisfies $h \leq \varepsilon/10$.

Note that, because we use a penalized approach, we do not have to mesh Ω_ε, which could be cumbersome and could possibly request elements of small size (comparable to the small size ε present in the geometry of Ω_ε). In addition, if we were working with a mesh of Ω_ε, we might face difficulties

with the oversampling variant of the MsFEM approach that we compare here with our approach. Indeed, edges of the oversampling domain may intersect the perforations. Properly defining the MsFEM basis functions in such a case would not be straightforward. For these two reasons, we consider a penalization approach.

5.1 Comparison with existing approaches

We solve (1) on the domain $\Omega = (0,1)^2$, with the right-hand side $f(x,y) = \sin\dfrac{\pi x}{2} \sin\dfrac{\pi y}{2}$, and we take B_ε the set of discs of radius 0.35ε periodically located on the regular grid of period $\varepsilon = 0.03$. For the reference solution, we use a mesh of size 1024×1024.

The approaches we compare our approach with are the following four respective approaches:

- the standard Q1 finite element method on the coarse mesh of size H. Of course, we do not expect that method to perform well for this multiscale problem and we only consider it as a "normalization".

- the MsFEM with linear boundary conditions. Although this method is now a bit outdated, it is still considered as the primary MsFEM approach, upon which all the other variants are built.

- the MsFEM with oscillatory boundary conditions. This variant (in the form presented in [18]) is restricted to the two-dimensional setting. It uses boundary conditions provided by the solution to the oscillatory ordinary differential equation obtained by taking the trace of the original equation on the edge considered. The approach performs fairly well on a number of cases, although it may also fail.

- the variant of MsFEM using oversampling. This variant is often considered as the "gold standard", although it includes a parameter (the oversampling ratio), the value of which should be carefully chosen. When this parameter is taken large, the method becomes (possibly prohibitively) expensive.

In addition, we consider for each of those approaches, and for our specific Crouzeix-Raviart type approach, two variants: one with, and the other without a specific enrichment of the basis set elements using bubble functions.

For all approaches but the Crouzeix-Raviart type approach that we propose, the bubble Ψ on the quadrangle Q is defined as the solution to

$$-\Delta\Psi = 1 \text{ on } Q \cap \Omega_\varepsilon, \quad \Psi = 0 \text{ on } \partial(Q \cap \Omega_\varepsilon).$$

For the Crouzeix-Raviart approach, the bubble function Ψ has been defined in Section 2.1 by (11).

Remark 12. *Other variants of the MsFEM approach have also been proposed, such as the Petrov-Galerkin variant with oversampling [19]. We do not consider this variant here, and refer to our previous work [21] for some elements of comparison (in a slightly different context).*

For a given mesh size H, the cost for computing the basis functions (offline stage) varies from one MsFEM variant to the other. However, for a fixed H, all methods without (respectively, with) bubble functions essentially share the same cost to solve the macroscopic problem on Ω (online stage). More precisely, for a given cartesian mesh, and when using variants including the bubble functions, there are 1.5 times more degrees of freedom in our Crouzeix-Raviart approach than in the three alternative MsFEM approaches mentioned above. Since a logarithmic scaling is used for the x-axis in the figures below, this extra cost does not change the qualitative conclusions we draw below.

The numerical results we have obtained in the regime where the meshsize H is of the order of, or larger than, the parameter ε are presented on Figure 4. For all values of the meshsize H, and for both L^2 and broken H^1 norms, a definite superiority of our approach over all other approaches is observed, and the interest of adding bubble functions to the basis set is, for each approach, also evident.

A side remark is the following. On Figure 4, we observe that, when using bubble functions, the error decreases as H increases. This might seem counterintuitive at first sight. Note however that, when H increases, the cost of computing each basis function increases, as we need to solve a local problem (discretized on a mesh of size h controlled by the value of ε) on a larger coarse element. In contrast to traditional FEM, increasing H does not correspond to reducing the overall computational cost. For MsFEM approaches, increasing H actually corresponds to decreasing the online cost but increasing the offline cost. The regime of interest is that of moderate

values of H, for which the offline stage cost is acceptable. We only show the right part of Figure 4 (corresponding to large values of H, leading to a prohibitively expensive offline stage) for the sake of completeness.
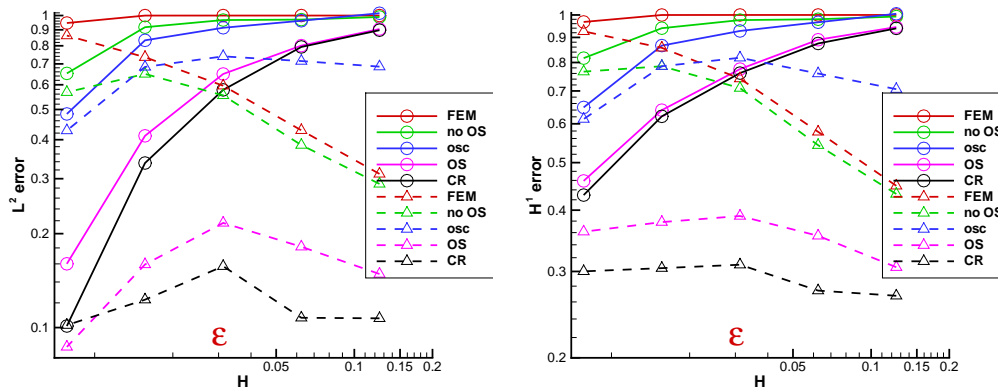
Figure 4: Relative (L^2, left, and H^1-broken, right) errors with various approaches in the regimes $H \simeq \varepsilon$ and $H \gtrsim \varepsilon$: FEM – the standard Q1 finite elements, no OS – MsFEM with linear boundary conditions, osc – MsFEM with oscillatory boundary conditions, OS – MsFEM with oversampling (where the size of the quadrangles used to compute the basis functions is $3H \times 3H$), CR – the MsFEM approach à la Crouzeix-Raviart we propose. Results for all these methods are represented by solid lines. The dashed lines correspond to the variants of these methods where we enrich the finite element spaces using bubble functions.

To get a better understanding of the approaches with bubble functions, we have run a series of tests in a regime different from that of Figure 4, where the meshsize H is of the order of, or larger than, the parameter ε. On Figure 5, we present results corresponding to the regime $H \ll \varepsilon$. This is performed only for the purpose of analyzing the behaviour of the methods and this is of course not the practical regime where we want to use MsFEM approaches. It is however useful to observe how the various numerical approaches behave in that regime. We consider the same problem as above, with $\varepsilon = 0.3$ instead of 0.03, and where the meshsize H ranges from $1/8$ to $1/128$, so that indeed H is smaller (and even much smaller) than ε. The reference solution is again computed on a mesh of size 1024×1024. As expected, we then observe that

all errors uniformly decrease when H decreases, in contrast to the situation displayed on Figure 4 and commented upon above. We then recover the classical behavior of numerical approaches in the limit of fine discretizations.
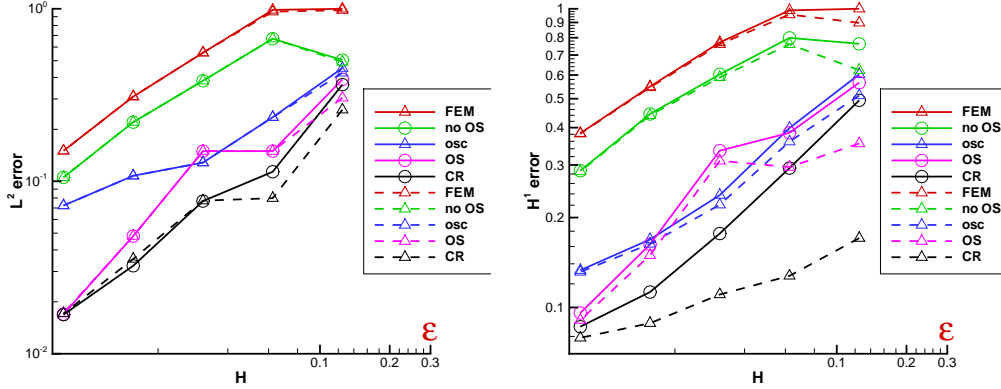
Figure 5: Relative (L^2, left, and H^1-broken, right) errors with the same approaches as on Figure 4, in the regime when $H \ll \varepsilon$.

For the sake of completeness, we have also considered another oversampling ratio for the MsFEM oversampling approach we compare our approach with. Recall indeed that, on Figures 4 and 5, we have considered an oversampling ratio equal to 3. We now additionally consider the method with an oversampling ratio equal to 2. Results are reported on Figure 6. As expected, the accuracy of MsFEM increases when the oversampling ratio increases. The artificial Dirichlet boundary conditions used to define basis functions are then further away from the relevant part of the mesh element, and their potentially poor behavior close to the boundary has a smaller influence. Of course, as the oversampling ratio increases, the cost of computing these basis functions increases. We observe that, with the MsFEM approach à la Crouzeix-Raviart we propose, we obtain a better accuracy (again both in H^1 and L^2 norms) than with the MsFEM approach that uses an oversampling ratio of 3 (i.e., that computes basis functions by solving local problems on quadrangles of size $3H \times 3H$).

Remark 13. *Figures 4, 5 and 6 show that, for any of the numerical approaches we have considered, the relative L^2 error is always smaller than*

34
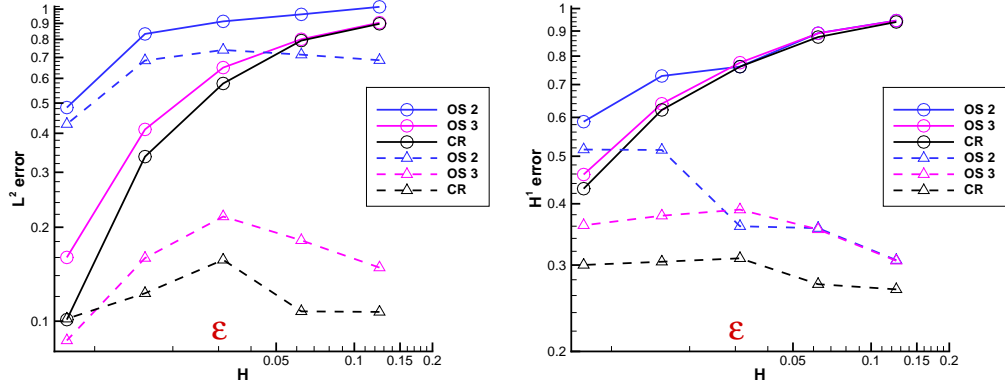
Figure 6: Relative (L^2, left, and H^1-broken, right) errors with various approaches (dashed lines: using bubble functions; solid lines: without bubble functions): OS – MsFEM with various oversampling ratios, CR – the MsFEM approach à la Crouzeix-Raviart we propose.

the relative H^1 error. The former presumably converges with a better rate (in terms of ε and H) than the latter, although establishing sharp L^2 error estimates for MsFEM-type approaches is quite involved (see e.g. [18]).

5.2 Robustness with respect to the location of the perforations

In this section and in the following one, we perform a series of tests with a different, specific purpose. As a major motivation for advocating our approach is the flexibility of Crouzeix-Raviart type finite elements in terms of boundary conditions, we expect our approach to be particularly effective (and therefore considerably superior to other approaches) when some edges of the mesh happen to intersect perforations of the domain. The more such intersections, the more important the difference. In order to check this expected behaviour, we design the following test.

We solve (1) on the domain $\Omega = (0,1)^2$, with a constant right-hand side $f = 1$, and we take B_ε the set of discs of radius 0.2ε periodically located on the regular grid of period $\varepsilon = 0.1$. We compute the reference solution, and consider 3 variants of MsFEM: the linear version, the oversam-

35

pling version and the Crouzeix-Raviart version. The last three approaches are implemented in the variant that includes bubble functions in the basis set and they are run on a mesh of size $H = 0.2$.

We now perform two sets of numerical experiments. They are identical except for what concerns the relative position of the mesh with the perforations. The difference between the two sets of tests is that, from one set of tests to the other one, the perforations are shifted by $\varepsilon/2$ in the directions x and y. In our Test 1, no edge intersects any perforation, while, on our Test 2, many edges actually intersect perforations. To some extent, the situation of Test 1 is the best case scenario (where as few edges as possible intersect the perforations) and the other situation is the worst case scenario.

The numerical solutions computed for each of the situations considered is shown on Figures 7 and 8, for Test 1 and Test 2 respectively. The numerical errors observed, computed both in L^2 and H^1-broken norms, are correspondingly displayed on Tables 1 and 2 respectively. More than the actual values obtained for each case, this is the trend of difference between Table 1 and Table 2 that is the practically relevant feature. A comparison between the two tables indeed show that, qualitatively and in either of the norms used for measuring the error, the linear version and the oversampling version of MsFEM are both much more sensitive to edges intersecting perforations than the Crouzeix-Raviart version of MsFEM. In particular, the gain of our approach with respect to the linear version of MsFEM is much higher in our Test 2 (which is, from the geometrical viewpoint, the worst case scenario) than in Test 1. This confirms the intuition of a better flexibility of our approach. This also allows for expecting a much better behaviour of that approach for nonperiodic multiscale perforated problems for which it is extremely difficult, practically, to avoid repeated intersections of perforations with mesh edges. This is confirmed by our numerical experiments of Section 5.3.

	L^2 error (%)	H^1 error (%)
MsFEM with linear conditions	16	32
MsFEM with oversampling	20	38
MsFEM à la Crouzeix-Raviart	9	24

Table 1: Numerical relative errors for Test 1
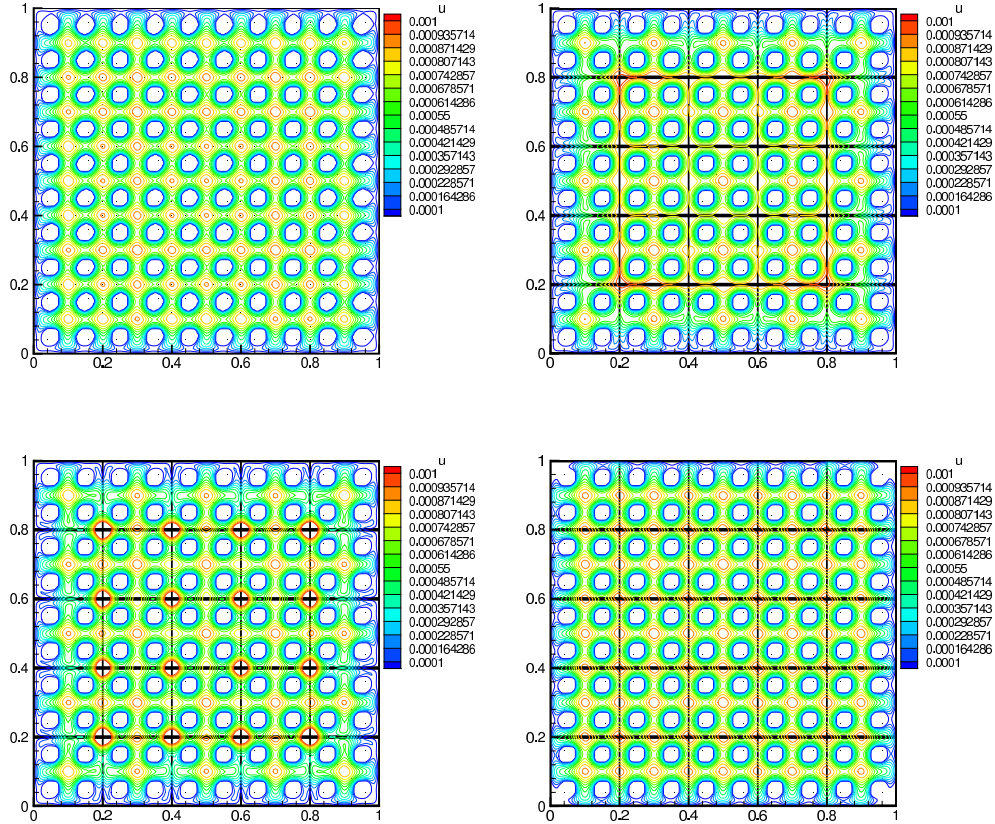
Figure 7: (Test 1) Left to right and top to bottom: Reference solution (on the mesh 200×200), MsFEM with linear boundary conditions, MsFEM with oversampling (where the size of the quadrangles used to compute the basis functions is $3H \times 3H$), proposed MsFEM à la Crouzeix-Raviart.
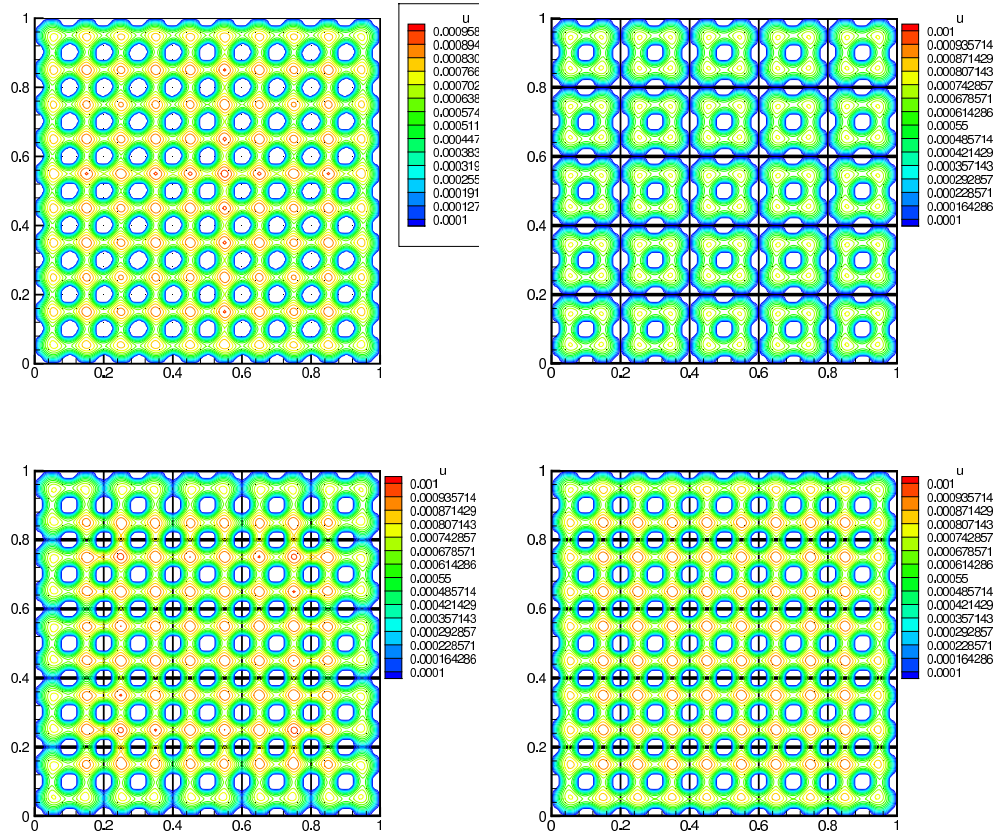
Figure 8: (Test 2) Left to right and top to bottom: Reference solution (on the mesh 200×200), MsFEM with linear boundary conditions, MsFEM with oversampling (where the size of the quadrangles used to compute the basis functions is $3H \times 3H$), proposed MsFEM à la Crouzeix-Raviart.

	L^2 error (%)	H^1 error (%)
MsFEM with linear conditions	28	52
MsFEM with oversampling	12	31
MsFEM à la Crouzeix-Raviart	9	27

Table 2: Numerical relative errors for Test 2

5.3   A test on a non-periodic geometry of perforations

A major motivation for using MsFEM approaches is to address non-periodic cases, for which homogenization theory does not provide any explicit approximation procedure. We have tested several such examples, two of them being shown on Figure 9. For each of them, the domain $\Omega = (0,1)^2$ is meshed using quadrangles of size H, with $1/128 \leq H \leq 1/8$. The reference solution is again computed on a mesh of size 1024×1024.
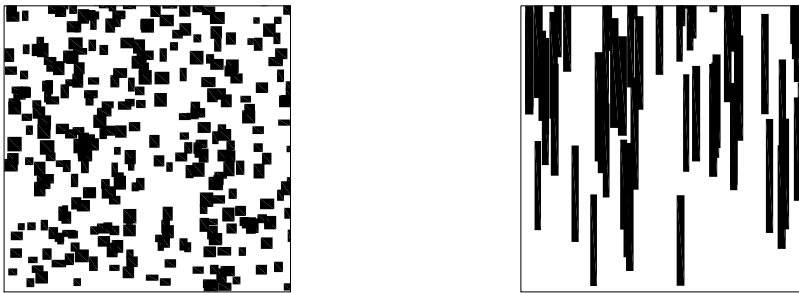
Figure 9: Two examples of domains with non-periodic perforations (represented in black). Perforations have a rectangular shape, with a center randomly located in $\Omega = (0,1)^2$ according to the uniform distribution. Left: perforations are made from 100 rectangles, the width and height of which are uniformly distributed between 0.02 and 0.05. Right: perforations are made from 60 rectangles, the width (resp. the height) of which is uniformly distributed between 0.02 and 0.04 (resp. 0.02 and 0.4).

Errors are shown on Figure 10 (resp. Figure 11) for the test-case shown on the left (resp. right) part of Figure 9 (we have obtained similar results for several other test cases not shown here for the sake of brevity). We again see

that our approach provides results at least as accurate as, and often more accurate than the MsFEM approach with oversampling on quadrangles of size $3H \times 3H$. Our approach outperforms all the other variants of MsFEM that we have tested. These results confirm the definite interest of the variant we introduce in this article.
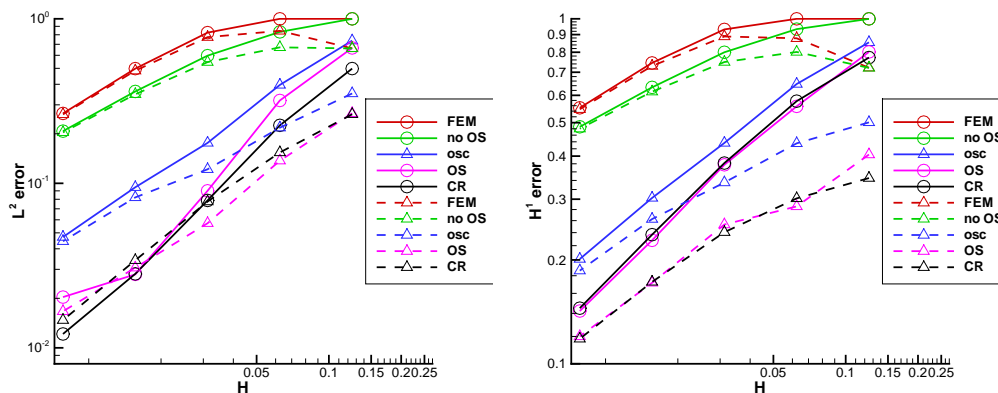
Figure 10: Relative (L^2, left, and H^1-broken, right) errors with the same approaches as on Figure 4 for the test-case shown on the left-part of Figure 9.

A   Technical proofs

We collect in this Appendix the proof of two technical results used in Section 4, namely the Poincaré inequality (23) and the homogenization result (21).
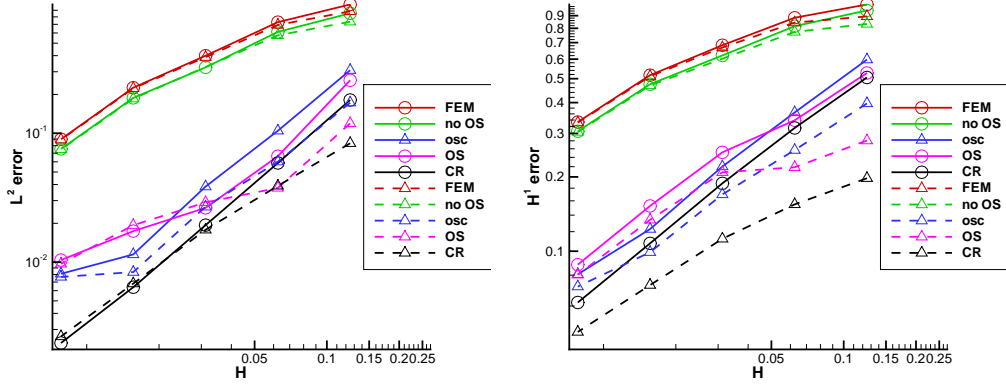
Figure 11: Relative (L^2, left, and H^1-broken, right) errors with the same approaches as on Figure 4 for the test-case shown on the right-part of Figure 9.

A.1 The Poincaré inequality in perforated domains

Consider the unit square $Y = (0,1)^d$ in dimension d, and some smooth perforation $B \subset Y$. There exists a constant $\mathcal{C} > 0$ such that, for any $\phi \in H^1(Y \setminus B)$ with $\phi = 0$ on ∂B, we have

$$\|\phi\|_{L^2(Y \setminus B)} \leq \mathcal{C} \|\nabla \phi\|_{L^2(Y \setminus B)}. \tag{56}$$

Let $Y_k^B := k + (Y \setminus B)$ be the perforated unit cell after translation by the vector $k \in \mathbb{Z}^d$. We scale Y_k^B by a factor ε and repeat this pattern periodically (with a period ε in all directions) for a finite number of times. We hence introduce

$$Q_\varepsilon = \bigcup_{k \in K} \left(\varepsilon Y_k^B \right), \quad K = \left\{ k \in \mathbb{Z}^d, \ a_i^- \leq k_i \leq a_i^+ \text{ for any } 1 \leq i \leq d \right\} \tag{57}$$

for some a_i^- and a_i^+ in $\mathbb{Z}$, that we can also write as

$$Q_\varepsilon = R_\varepsilon \setminus P_\varepsilon,$$

where R_ε is the quadrangle $R_\varepsilon = \bigcup_{k \in K} \left(\varepsilon(k + Y) \right)$ and P_ε is the set of perforations $P_\varepsilon = \bigcup_{k \in K} \left(\varepsilon(k + B) \right)$. Summing the inequality (56) for all cells and next

41

scaling the geometry, we obtain that, for any $\phi \in H^1(R_\varepsilon \setminus P_\varepsilon)$ with $\phi = 0$ on ∂P_ε, we have

$$\|\phi\|_{L^2(R_\varepsilon \setminus P_\varepsilon)} \leq \mathcal{C}\varepsilon \|\nabla\phi\|_{L^2(R_\varepsilon \setminus P_\varepsilon)} \tag{58}$$

where $\mathcal{C}$ is the same constant as in (56).

Consider now $\phi \in H_0^1(\Omega_\varepsilon)$. There exists a set K of the form (57) such that $\Omega_\varepsilon \subset Q_\varepsilon$ (it is sufficient to include Ω_ε into a sufficiently large perforated quadrangle). We now introduce $\overline{\phi}$, defined on Q_ε by

$$\overline{\phi} = \phi \text{ on } \Omega_\varepsilon, \quad \overline{\phi} = 0 \text{ otherwise,}$$

and readily see that $\overline{\phi} \in H^1(Q_\varepsilon)$ and $\overline{\phi} = 0$ on ∂P_ε. The function $\overline{\phi}$ thus satisfies (58). We hence obtain

$$\|\phi\|_{L^2(\Omega_\varepsilon)} = \left\|\overline{\phi}\right\|_{L^2(R_\varepsilon \setminus P_\varepsilon)} \leq \mathcal{C}\varepsilon \left\|\nabla\overline{\phi}\right\|_{L^2(R_\varepsilon \setminus P_\varepsilon)} = \mathcal{C}\varepsilon \|\nabla\phi\|_{L^2(\Omega_\varepsilon)}.$$

This completes the proof of (23).

A.2 Homogenization result

In this section, we prove (21). To do so, we actually do not use (18). The proof below actually provides an alternative proof of (18) (see Remark 14 below).

Let η^ε be a smooth function on $\overline{\Omega}$ that vanishes on $\partial\Omega$, satisfies $0 \leq \eta^\varepsilon(x) \leq 1$ on $\overline{\Omega}$ and is equal to 1 in $\omega_\varepsilon = \{x \in \Omega \text{ s.t. } \mathrm{dist}(x, \partial\Omega) > \varepsilon\}$. Using the fact that Ω is smooth, it is easy to see that such a function can be constructed for each $\varepsilon > 0$ and we can suppose that it satisfies

$$\|\eta^\varepsilon\|_{L^\infty(\Omega)} \leq C, \quad \|1 - \eta^\varepsilon\|_{L^2(\Omega)} \leq C\sqrt{\varepsilon},$$
$$\|\nabla\eta^\varepsilon\|_{L^\infty(\Omega)} \leq \frac{C}{\varepsilon}, \quad \|\nabla\eta^\varepsilon\|_{L^2(\Omega)} \leq \frac{C}{\sqrt{\varepsilon}}, \quad \left\|\nabla^2\eta^\varepsilon\right\|_{L^2(\Omega)} \leq \frac{C}{\varepsilon^{3/2}} \tag{59}$$

for some universal constant $C > 0$. Set $\phi = u^\varepsilon - \varepsilon^2 w_\varepsilon f \eta^\varepsilon$, where $w_\varepsilon(x) = w(x/\varepsilon)$, with w the solution to (19). We compute

$$\begin{aligned}
-\Delta\phi &= f + \varepsilon^2\Delta(w_\varepsilon f \eta^\varepsilon) \\
&= f + (\Delta w)_\varepsilon f \eta^\varepsilon + 2\varepsilon(\nabla w)_\varepsilon \cdot \nabla(f \eta^\varepsilon) + \varepsilon^2 w_\varepsilon \Delta(f \eta^\varepsilon) \\
&= f(1 - \eta^\varepsilon) + 2\varepsilon(\nabla w)_\varepsilon \cdot \nabla(f \eta^\varepsilon) + \varepsilon^2 w_\varepsilon \Delta(f \eta^\varepsilon)
\end{aligned}$$

on Ω_ε, where we have used (1) in the first line and the fact that $-\Delta w = 1$ on $Y \setminus B$ in the last line. Using the regularity (20) of w and the properties (59) of η^ε, we deduce that

$$
\begin{aligned}
& \| - \Delta\phi\|_{L^2(\Omega_\varepsilon)} \\
\leq\ & \|f\|_{L^\infty(\Omega)} \|1 - \eta^\varepsilon\|_{L^2(\Omega)} \\
& + 2\varepsilon \|\nabla w\|_{L^\infty} \left(\|f\|_{L^\infty(\Omega)} \|\nabla\eta^\varepsilon\|_{L^2(\Omega)} + \|\nabla f\|_{L^2(\Omega)} \|\eta^\varepsilon\|_{L^\infty(\Omega)} \right) \\
& + \varepsilon^2 \|w\|_{L^\infty} \left(\|f\|_{L^\infty(\Omega)} \|\Delta\eta^\varepsilon\|_{L^2(\Omega)} + 2\|\nabla f\|_{L^2(\Omega)} \|\nabla\eta^\varepsilon\|_{L^\infty(\Omega)} \right. \\
& \qquad\qquad\qquad \left. + \|\Delta f\|_{L^2(\Omega)} \|\eta^\varepsilon\|_{L^\infty(\Omega)} \right) \\
\leq\ & C\sqrt{\varepsilon}\,\mathcal{N}(f), \hspace{5cm} (60)
\end{aligned}
$$

where $\mathcal{N}(f)$ is defined by (22).

We now notice that u^ε and $w_\varepsilon \eta^\varepsilon$ vanish on $\partial\Omega_\varepsilon$, hence $\phi = 0$ on $\partial\Omega_\varepsilon$. An integration by parts thus yields

$$
\int_{\Omega_\varepsilon} |\nabla\phi|^2 = \int_{\Omega_\varepsilon} (-\Delta\phi)\,\phi \leq C\sqrt{\varepsilon}\,\mathcal{N}(f)\,\|\phi\|_{L^2(\Omega_\varepsilon)}. \tag{61}
$$

Inserting (23) in (61), we obtain $|\phi|_{H^1(\Omega_\varepsilon)} \leq C\varepsilon^{3/2}\mathcal{N}(f)$. We conclude by using the triangle inequality

$$
\left| u^\varepsilon - \varepsilon^2 w\left(\frac{\cdot}{\varepsilon}\right) f \right|_{H^1(\Omega_\varepsilon)} \leq |\phi|_{H^1(\Omega_\varepsilon)} + \varepsilon^2 \left| w\left(\frac{\cdot}{\varepsilon}\right) f(1 - \eta^\varepsilon) \right|_{H^1(\Omega_\varepsilon)},
$$

where both terms in the above right-hand side are bounded by $C\varepsilon^{3/2}\mathcal{N}(f)$. This yields the desired bound (21).

Remark 14. *Note that if f vanishes on $\partial\Omega$, we can take $\eta^\varepsilon \equiv 1$ and (60) is replaced by*

$$
\| - \Delta\phi\|_{L^2(\Omega_\varepsilon)} \leq C\varepsilon\,\mathcal{N}(f).
$$

Following the same steps as above, we then recover the bound (18).

References

[1] P. Angot, C.-H. Bruneau and P. Fabrie, *A penalization method to take into account obstacles in incompressible viscous flows*, Numer. Math., 81:497-520, 1999.

[2] T. Arbogast, *Mixed multiscale methods for heterogeneous elliptic problems*, in *Numerical Analysis of Multiscale Problems*, I.G. Graham, T.Y. Hou, O. Lakkis and R. Scheichl, eds., Lecture Notes in Computational Science and Engineering, vol. 83, Springer, pp. 243-283, 2011.

[3] A. Bensoussan, J.-L. Lions and G. Papanicolaou, *Asymptotic analysis for periodic structures*, Studies in Mathematics and its Applications, 5. North-Holland Publishing Co., Amsterdam-New York, 1978.

[4] S.C. Brenner and L.R. Scott, *The mathematical theory of finite element methods*, 3rd edition, Springer, 2008.

[5] L. Carballal Perdiz, *Etude d'une méthodologie multiéchelles appliquée à différents problèmes en milieu continu et discret* (in french), Thèse de l'Université Toulouse III, 2010, http://thesesups.ups-tlse.fr/1170/.

[6] D. Cioranescu, P. Donato and R. Zaki, *Periodic unfolding and Robin problems in perforated domains*, C.R. Acad. Sci. Paris, 342:469-474, 2006.

[7] D. Cioranescu and F. Murat, *A strange term coming from nowhere*, in *Topics in the Mathematical Modelling of Composite Materials*, A. Cherkaev and R. Kohn, eds., Progress in Nonlinear Differential Equations and their Applications, vol. 31, Birkhäuser, pp. 45-93, 1997.

[8] D. Cioranescu and J. Saint Jean Paulin, *Homogénéisation dans des ouverts à cavités*, C.R. Acad. Sci. Paris, 284:857-860, 1977.

[9] M. Crouzeix and P.-A. Raviart, *Conforming and nonconforming finite element methods for solving the stationary Stokes equations I*, RAIRO, 7(3):33-75, 1973.

[10] Y. Efendiev and T. Hou, *Multiscale Finite Element method*, Theory and applications. Surveys and Tutorials in the Applied Mathematical Sciences, 4. Springer, New York, 2009.

[11] B. Engquist and P. Souganidis, *Asymptotic and numerical homogenization*, Acta Numerica 17, 2008.

[12] A. Ern and J.-L. Guermond, *Theory and practice of Finite Elements*, Applied Mathematical Sciences, vol. 159, Springer, 2004.

[13] D. Gérard-Varet and N. Masmoudi, *Homogenization in polygonal domains*, J. Eur. Math. Soc., 13:1477-1503, 2011.

[14] D. Gérard-Varet and N. Masmoudi, *Homogenization and boundary layers*, Acta Math., 209:133-178, 2012.

[15] D. Gilbarg and N.S. Trudinger, *Elliptic partial differential equations of second order*, reprint of the 1998 ed., Classics in Mathematics, Springer, 2001.

[16] P. Henning and M. Ohlberger, *The heterogeneous multiscale finite element method for elliptic homogenization problems in perforated domains*, Numer. Math., 113(4):601-629, 2009.

[17] U. Hornung, *Homogenization and Porous Media*, Interdisciplinary Applied Mathematics, vol. 6, Springer, 1997.

[18] T.Y. Hou, X.-H. Wu and Z. Cai, *Convergence of a multiscale finite element method for elliptic problems with rapidly oscillating coefficients*, Maths. of Comp., 68(227):913-943, 1999.

[19] T.Y. Hou, X.-H. Wu and Y. Zhang, *Removing the cell resonance error in the multiscale finite element method via a Petrov-Galerkin formulation*, Communications in Mathematical Sciences, 2(2):185-205, 2004.

[20] V.V. Jikov, S.M. Kozlov and O.A. Oleinik, *Homogenization of differential operators and integral functionals*, Springer-Verlag, 1994.

[21] C. Le Bris, F. Legoll and A. Lozinski, *MsFEM à la Crouzeix-Raviart for highly oscillatory elliptic problems*, Chinese Annals of Mathematics, Series B, vol. 34 (1), 113-138 (2013).

[22] J.-L. Lions, *Asymptotic expansions in perforated media with a periodic structure*, Rocky Mountain J. of Maths., 10(1):125-140, 1980.